Mathematical Modelling of Platelet Signalling Pathways

Mark Payne

October 12, 2009

This dissertation is submitted to the Department of Mathematics in partial fulfilment of the requirements for the degree of Master of Science.

Abstract

In this dissertation we outline a mathematical model of the collagen – glycoprotein VI platelet signalling pathway. Platelets are small annucleate cell that play an important part in haemostasis. Disorders in platelet activation can be the cause of many serious disorders.

Starting from a detailed biological diagram we construct a simple schematic model of the collagen - glycoprotein VI pathway. From this model we extract the main reaction equations. Using the Law of Mass Action we change the reaction equations to a system of non-linear ordinary differential equation which we then reduce further. After non–dimensionalising, we solve these equations numerically and find that the model produces the desired rise in calcium within the platelet cytosol. We perform a sensitivity analysis on the model finding certain parmeters significantly affect the model more than others.

We then improve the model adding IP_3 and DAG recycling as well as the movement of calcium from the cytosol into the dense tubular structure of the platelet. Again we performed sensitivity analysis, explaining differences between the two models. Lastly we compare our model output to experimental data.

Acknowledgements

I would like to thank my supervisors Dr. Marcus Tindall and Professor Peter Grindrod as well as Dr. Mike Fry and Dr. Chris Jones for their support during writing this dissertation. I would also like to thank the ESPRC as without their funding my completion of this course would not have been possible. Lastly I would like to thank my friends Tom Holdstock and Laura Stewart for keeping me sane during my time at Reading.

Declaration

I confirm that this is my own work, and the use of all material from other sources has been properly and fully acknowledged.

Signed....................... Date.......................

List of Figures

Contents

Chapter 1

Introduction

The work presented in this dissertation relates to mathematically modelling chemical pathways within platelet cells. Platelets are small anucleate cells that are found within the blood, used to repair damage and stop bleeding by forming clots (thrombus). Disruption in platelet function can lead to venal thromboembolism (VTE) and other disorders. VTE is a serious condition which can lead to heart attacks or pulmonary embolism.

VTE is the blocking of a vein by the aggregation of a large number of platelets (or thrombus). It is possible for this clot to break away and lodge within vital organs, such as the lungs or the heart, obstructing blood flow. This obstruction of blood flow in the heart can lead to heart attacks, while in the lungs it stops the uptake of oxygen by the blood leading to a pulmonary embolism. The American Heart Association, [1] report that 100 people per $100,000$ are diagnosed with thromboembolism for the first time each year in the United States. Of the $200,000$ new cases diagnosed annually it is reported 30% die within 30 days with another 30% developing recurring VTE within 10 years.

This means that an understanding of platelet function is important as it could not only reveal possible causes for VTE and other disorders, but also

help develop new medications to combat the disease.

1.1 Platelets and Haemostasis

Haemostasis is the physiological response to stop bleeding and repair blood vessels. This involves changing the blood from a fluid to a solid state to block any breach in the wall of blood vessels. Haemostasis has three main components; vascular spasm, platelet formation and blood coagulation.

Platelets and fibrogen are the main factors in the formation of a plug and blood coagulation. The aim of plug formation is to block any breach in the vessel walls to stop blood escaping and restore the normal flow. Blood coagulation then helps repair the vessel walls.

The thrombus formation process can be seen in Figure 1.1. The process starts when collagen in the vessel wall becomes exposed through damage or injury. When the platelet comes into contact with the collagen it becomes active, changing shape and binding to the injury site using the von Willebrand factor protein. The collagen initiates chemical pathways within the platelet, some of which can be seen in Figure 1.2, which ultimately triggers the secretion of thrombin which activates other platelets and causes aggregation. A fibrin mesh is then formed between platelets resulting in a thrombus.

Malfunctions in platelets can have varied results. Thrombi can be brittle and easily broken off by blood flow causing them to travel downstream towards major organs. Too large thrombi can block vessels restricting blood flow, reducing the supply of oxygen around the body, while inactive platelets can lead to a lack of thrombus formation leading to bleeding disorders.

Figure 1.1: The thrombus formation process, from [2]

Figure 1.2: A schematic diagram indicating th collagen activated chemical pathways within the platelet, from [4]

1.1.1 Cell Signaling and the Collagen – Glycoprotein VI Receptor Signaling Pathway

Cells need to be able to react to changes in their surrounding environment and behave accordingly. To do this they use, in most cases several, chemical cascades called cell signalling pathways.

These pathways start with a receptor protein. Certain external chemicals, called receptor ligands, bind and activate these proteins. This leads to a series of internal chemical reactions that give an output such as a change in cellular behaviour or a secretion of a chemical in the extracellular space.

The chemical pathway of interest throughout this dissertation is the Collagen – Glycoprotein VI receptor (GPVI) signaling pathway. This is an important pathway as it activates at a vessel injury site.

In this pathway it is movement of calcium (Ca^{2+}) between two areas of the platelet, the dense tubular structure (DTS) and cytosol, which affects the platelets behaviour. The pathway begins with collagen binding with GPVI, this causes the phosphorylation of SYK which in turn triggers the phosphorylation of of LAT. These interactions causes a chain of reactions that phosphorylate and activate protein further downstream which eventually leads to the transferrence of Ca^{2+} from the DTS of the platelet to it's cytosol. This leads to an increase in integrin secretion.

The mathematical modelling of cell signaling pathways within platelet cells has only been considered recently, although in other cell types it has been widely applied. The mathematical modelling of such pathways is important to help form an understanding of the affect of any changes within the pathway, elucidating biological complexity.

The purpose of this dissertation is to develop a system of differential equations which mathematical model the Collagen – GPVI signaling pathway. Once a suitable system has been developed we carry out analysis of

the model, such as it's sensitivity to parameter change and whether a steady state solution exists. The results of the model, the analysis and any possible further work are then discussed.

1.2   Literature Review

Mathematical models of blood coagulation mainly fall into two categories, either they focus on the chemical pathways that trigger thrombus formation or their development.

Purvis et al. [12] formulated a molecular signalling model of platelet phosphoinositide and calcium regulation during homeostatis and $P2Y_1$ activation. The network model was informed by 23 peer-reviewed studies spanning three decades of platelet research. The model consists of four distinct signalling 'modules'; Ca^{2+} release and uptake, phosphoinositide metabolism, $P2Y_1$ G-protein signalling and protein kinase C regulation of phospholipase C–β. These four modules were then interlinked to become the full model. Non–linear ordinary differential equations were used to model the network modules and simulations were performed using the SBToolbox for MATLAB. The results of this model displayed similar behaviour to what was observed in experimentally. The model also fulfilled the requirements of of maintaining homeostasis under resting conditions while being capable of generating an activation response in the presence of sufficiently high antagonist concentration.

Xu et al. [15] developed a multiscale model of thrombus development within a single blood vessel. The model included the Navier-Stokes and advection-diffusion equation to simulate the blood flow and the chemicals within it, respectively. Cell movement and cell–cell interactions were modelled using the cellular Potts model, which is a stochastic model, with flow and adhesion energy. While kinetic equations modelled fibril generation and

thrombin generation at the sub-cellular level. The model was then used to simulate the development of a thrombus. Xu et al. [15] found that vortical flow created during the early formation of the thrombus effected it's later growth as some activated platelets were flushed back by the rolling flow to the back of the thrombus (opposing end to the direction of flow). The size of the thrombus in the simulation and it's dependence on the rate of blood flow quantitatively agreed with experimental data. The model also predicted heterogeneity within the thrombus; blood cells trapped within the thrombus, could lead to structural instability.

Pivkin et al. [11] studied the effect of blood flow velocity and the role of activation delay time on the growth and formation of thrombi. They developed a 3–D model of blood flow in a 50μm diameter straight tube, 500μm long. Several different steady blood flow rates were used and platelets were considered to be uniformly distributed in the inflow. Simulation results were compared to experimental data found previously. Pivkin and colleagues then extended the simulation to investigate the effect of the pulsatility of blood flow. They found the simulation predicted thrombi growth with shapes and patterns similar to those observed experimentally. Thrombi formed under the same flow conditions were found to have a varied time for small-growth of the thrombus. However, this small-growth time had little effect on the thrombus's major growth, which happens at an exponential rate. It was also noted that the exponential growth rate rose initially proportionally to the flow rate to a maximum and then fell as the flow rate increased further. This was in agreement with experimental results. When investigating pulsatility they found this had very little affect on thrombi growth and produced similar results to the steady flow results.

Xu et al. [14] proposed a non-linear dynamic model to explain bleeding tendency due to defficiency of certain proteins. They considered all proteins in insufficient amounts which cause bleeding as well as taking into account the role of platelet surface in blood coagulation. The model views coagu-

lation in three distinct steps; the initiation stage, the activation stage and the propagation stage. In the initiation stage a protein, tissue factor, is exposed to blood-born enzymes at the injury site which leads to small amounts of thrombin being activated. The amplification stage is when platelets are activated and provide a surface on which activated factors, or enzymes, to assemble and form complexes. In the propogation stage, large scale thrombin production takes place on the surface of the platelet if enough complexes are formed. A system of linked differential equations form the model and stability analysis was carried out. Results showed that deficiencies in certain proteins within the blood reduces the rate of thrombin generation resulting in bleeding tendency which is consistent with experimental findings.

Morbiducci et al. [9] looked at how flow patterns and stresses affected platelet activation in mechanical heart valves. Many patients who undergo mechanical heart valve implatation sustain thromboembolic complications and thrombus deposition. The model used was one originally developed for the evaluation of mechanical damage to red blood cells but was adapted for the assessment of platelet activation state under dynamic loading conditions. The simulation was carried out with 3960 idealised platelet-like particles that were released at four different phases during the hearts contractions at a distance of 2mm from the valve. From the model they confirmed, through statistical analysis, that platelet activation is dependent on the phase of the cardiac cycle. They also found that the vorticity created by the valves played a role in the activation of platelets.

1.3   Outline

In this dissertation we formulate a model for the collagen–GPVI pathway. In chapter 2 we discuss the development of the model. We simplify the biological model of protein–protein intracellular reactions and identify the

reaction equations. We then form a system of ordinary differential equations which we non-dimensionalise and then solve numerically. We then carry out sensitivity analysis of the model. The method used for our analysis is outlined and carried out. The results of our sensitivity analysis are then presented and discussed.

We extend the model more in chapter 3. The recycling of IP_3 and DAG to PI and also the movement of calcium from the cytosol to the DTS are added. This is done by adding new reaction equations which leads to a new system of differential equations. This system is then non–dimensionalised and solved with differences between the two models being discussed. Sensitivity analysis is then carried out and the model is tested without the presence of collagen as a check. The model is then compared to experimental data that has been supplied to us with possible reasons for differences outlined.

In chapter 4 we draw conclusions from our work and outline future work.

Chapter 2

A Model of Platelet Signalling

In this chapter we develop a mathematical model of the Collagen – GPVI pathway as shown in Figure (2.1). We removed the non-essential parts of the pathway, and simplified many of the steps to obtain the pathway in Figure (2.2). From this simplified model the series of protein reaction equations (2.1) – (2.18) could be obtained.

$$R_0 + C \xrightarrow{k_1} R_1 \tag{2.1}$$

$$R_1 \xrightarrow{k_2} R_2 \tag{2.2}$$

$$SYK + R_2 \xrightarrow{k_3} SYK \cdot R_2 \xrightarrow{k_4} SYK_P \cdot R_2 \tag{2.3}$$

$$LAT + SYK_P \cdot R_2 \xrightarrow{k_5} LAT_P + SYK_P \cdot R_2 \tag{2.4}$$

$$LAT_P + SYK_P \cdot R_2 \xrightarrow{k_6} LAT_{PP} \tag{2.5}$$

$$LAT_{PP} + PI3K \xrightarrow{k_7} PI3K^* \cdot LAT_{PP} \tag{2.6}$$

$$PI3K^* \cdot LAT_{PP} + PIP_2 \xrightarrow{k_8} PIP_3 + PI3K^* \cdot LAT_{PP} \tag{2.7}$$

$$PIP_3 + PTEN \xrightarrow{k_9} PIP_2 + PTEN \tag{2.8}$$

$$PIP_3 + BtK \xrightarrow{k_{10}} PIP_3 \cdot BtK^* \tag{2.9}$$
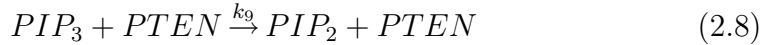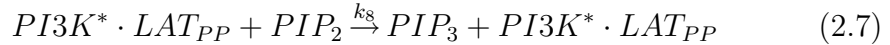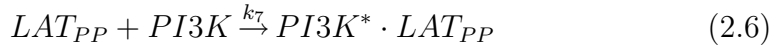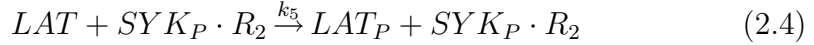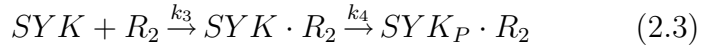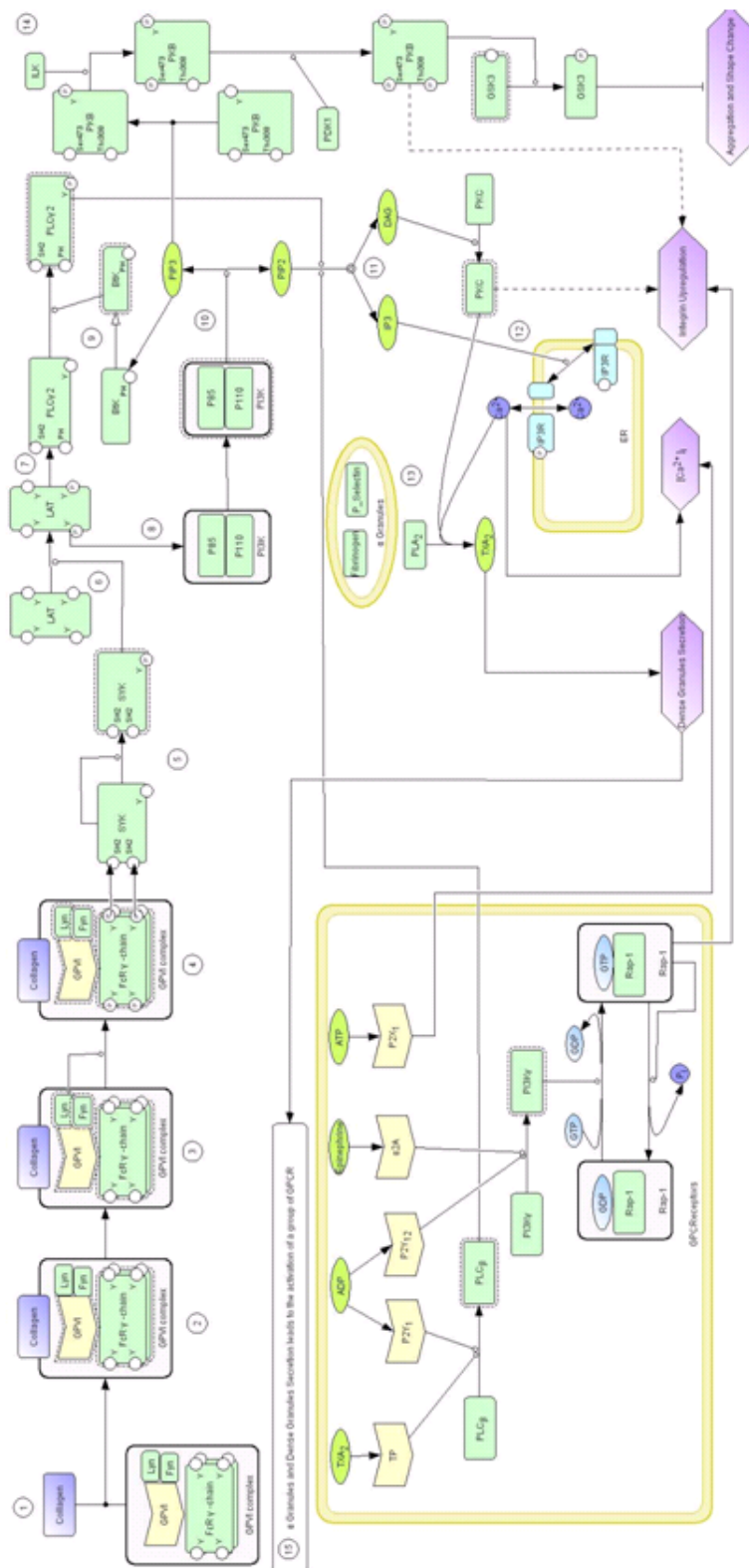
Figure 2.1: Biological Model of the Collagen − GPVI pathway from [5].

Figure 2.2: Schematic Diagram of Model.

$$LAT_P + PLC\gamma_2 \xrightarrow{k_{11}} LAT_P \cdot PLC\gamma_2 \tag{2.10}$$

$$LAT_{PP} + PLC\gamma_2 \xrightarrow{k_{12}} LAT_{PP} \cdot PLC\gamma_2 \tag{2.11}$$

$$PIP_3 \cdot BtK^* + LAT_P \cdot PLC\gamma_2 \xrightarrow{k_{13}} PIP_3 \cdot BtK^* + LAT_P \cdot PLC\gamma_{2P} \tag{2.12}$$

$$PIP_3 \cdot BtK^* + LAT_{PP} \cdot PLC\gamma_2 \xrightarrow{k_{14}} PIP_3 \cdot BtK^* + LAT_{PP} \cdot PLC\gamma_{2P} \tag{2.13}$$

$$LAT_P \cdot PLC\gamma_{2P} + PIP_2 \xrightarrow{k_{15}} LAT_P \cdot PLC\gamma_{2P} + IP_3 + DAG \tag{2.14}$$

$$LAT_{PP} \cdot PLC\gamma_{2P} + PIP_2 \xrightarrow{k_{16}} LAT_{PP} \cdot PLC\gamma_{2P} + IP_3 + DAG \tag{2.15}$$

$$PI \underset{k_{-17}}{\overset{k_{17}}{\rightleftharpoons}} PIP \underset{k_{-18}}{\overset{k_{18}}{\rightleftharpoons}} PIP_2 \tag{2.16}$$

$$IP_3 + IP_{3RC} \xrightarrow{k_{19}} IP_3 \cdot IP_{3RO} \tag{2.17}$$

$$Ca^{(1)} + IP_3 \cdot IP_{3RO} \xrightarrow{k_{20}} IP_3 \cdot IP_{3RO} + Ca^{(2)} \tag{2.18}$$

Equation (2.1) is the binding of collagen to the unbound receptor, R_0, to

form the inactive bound receptor, R_1, which then becomes active in (2.2). (2.3) shows the enzyme SYK then binds to the active receptor R_2 and auto-phosphorylating. The complex $SYK \cdot R_2$ then plays a role in the auto-phosphorylation of LAT and the phosphorylation of LAT_P in equations (2.4) and (2.5). LAT_{PP} forms a complex with $PI3K$ which then becomes active in equation (2.6). Equations (2.7), (2.8) and (2.16) form the lipid cycle. The lipid PIP_3 forms a complex with the enzyme BtK with then activates in (2.9). LAT_P and LAT_{PP} form complexes with $PLC\gamma_2$ in (2.10) and (2.11) which then auto-phosphorylate in (2.12) and (2.13). $LAT_P \cdot PLC\gamma_{2P}$ and $LAT_P \cdot PLC\gamma_{2P}$ then react with PIP_2 to release IP_3 and DAG, as shown in (2.14) and (2.15). IP_3 then opens the ion channel IP_{3RO} in (2.17) to allow the calcium transfer in (2.18).

In obtaining these reaction equations we made the assumption that, for the most part, only the forward reactions played a meaningful part in the platelet pathway. This assumption is appropriate as once the platelet is activated the forward reactions must be dominant to produce the increased concentration of Ca^{2+} within the cytosol. We also assume that the proteins within the platelet are spatially homogeneous, therefore the spatial concentration of the proteins can be ignored. In our model the collagen concentration remains constant, this is due to the injury site keeps emmiting collagen and it is used by the platelet.

These reaction equations could then be transformed into a system of non-linear differential equations using the Law of Mass Action. The Law of Mass Action [10] states that the rate of a reaction is proportional to the product of the concentration of the reactants. A source term was added to the equation for P to stop the concentration of lipids becoming zero. The system of

differential equations, using the variables in Table 2.1, is listed below.

$$\frac{dR_0^c}{dt} = -k_1 R_0^c C \tag{2.19}$$

$$\frac{dR_1^c}{dt} = k_1 R_0^c C - k_2 R_1^c \tag{2.20}$$

$$\frac{dR_2^c}{dt} = k_2 R_1^c - k_3 S R_2^c \tag{2.21}$$

$$\frac{dS}{dt} = -k_3 S R_2^c \tag{2.22}$$

$$\frac{dv_1}{dt} = k_3 S R_2^c - k_4 v_1 \tag{2.23}$$

$$\frac{dv_2}{dt} = k_4 v_1 - k_6 L_P v_2 \tag{2.24}$$

$$\frac{dL}{dt} = -k_5 L v_2 \tag{2.25}$$

$$\frac{dL_P}{dt} = k_5 L v_2 - k_6 L_P v_2 - k_{11} L_P P_\gamma \tag{2.26}$$

$$\frac{dL_{PP}}{dt} = k_6 L_P v_2 - k_7 L_{PP} P_K - k_{12} L_{PP} P_\gamma \tag{2.27}$$

$$\frac{dP_K}{dt} = -k_7 L_{PP} P_K \tag{2.28}$$

$$\frac{dv_3}{dt} = k_7 L_{PP} P_K \tag{2.29}$$

$$\frac{dP}{dt} = -k_{17} P + k_{-17} P_1 + \frac{k_E}{k_s + P} \tag{2.30}$$

$$\frac{dP_1}{dt} = k_{17} P - k_{18} P_1 - k_{-17} P_1 + k_{-18} P_2 \tag{2.31}$$

$$\frac{dP_2}{dt} = -k_8 v_3 P_2 + k_9 P_3 P^{10} - k_{15} v_7 P_2 - k_{16} v_8 P_2$$
$$+ k_{18} P - k_{-18} P_2 \tag{2.32}$$

$$\frac{dP_3}{dt} = k_8 v_3 P_2 - k_9 P_3 P^{10} - k_{10} P_3 B \tag{2.33}$$

$$\frac{dB}{dt} = -k_{10}P_3B \tag{2.34}$$

$$\frac{dv_4}{dt} = k_{10}P_3B \tag{2.35}$$

$$\frac{dP_\gamma}{dt} = -k_{11}L_PP_\gamma - k_{12}L_{PP}P_\gamma \tag{2.36}$$

$$\frac{dv_5}{dt} = k_{11}L_PP_\gamma - k_{13}v_4v_5 \tag{2.37}$$

$$\frac{dv_6}{dt} = k_{12}L_{PP}P_\gamma - k_{14}v_4v_6 \tag{2.38}$$

$$\frac{dv_7}{dt} = k_{13}v_4v_5 \tag{2.39}$$

$$\frac{dv_8}{dt} = k_{14}v_4v_6 \tag{2.40}$$

$$\frac{dI}{dt} = k_{15}v_7P_2 + k_{16}v_8P_2 - k_{19}II_{RC} \tag{2.41}$$

$$\frac{dD}{dt} = k_{15}v_7P_2 + k_{16}v_8P_2 \tag{2.42}$$

$$\frac{dI_{RC}}{dt} = -k_{19}II_{RC} \tag{2.43}$$

$$\frac{dv_9}{dt} = k_{19}II_{RC} \tag{2.44}$$

$$\frac{dCa_1}{dt} = -k_{20}v_9Ca_1 \tag{2.45}$$

$$\frac{dCa_2}{dt} = k_{20}v_9Ca_1. \tag{2.46}$$

These equation are to be solved with the initial conditions as in tables (2.2) and (2.3).

Certain proteins within our system are conserved as is now shown. Addition of equations (2.25), (2.26), (2.27), (2.29), (2.37), (2.38), (2.39) and (2.40) leads to,

$$\frac{dL}{dt} + \frac{dL_P}{dt} + \frac{dL_{PP}}{dt} + \frac{dv_3}{dt} + \frac{dv_5}{dt} + \frac{dv_6}{dt} + \frac{dv_7}{dt} + \frac{dv_8}{dt} = 0.$$

Table 2.1: Table of Variables

Notation	Meaning
C	Concentration of collagen.
R_0	Unbound GPVI receptors.
R_1	Bound, inactive GPVI receptors.
R_2	Bound, active GPVI receptors.
R_0^c	Concentration of R_0.
R_1^c	Concentration of R_1.
R_2^c	Concentration of R_2.
S	Concentration of SYK.
v_1	Concentration of the complex $SYK \cdot R_2$.
v_2	Concentration of the complex of phosphorylated SYK ($SYK_P \cdot R_2$).
L	Concentration of LAT.
L_P	Concentration of phosphorylated LAT (LAT_P).
L_{PP}	Concentration of twice phosphorylated LAT (LAT_{PP}).
P_K	Concentration of $PI3K$.
v_3	Concentration of complex of active $PI3K$ ($PI3K^* \cdot LAT_{PP}$).
P	Concentration of PI.
P_1	Concentration of PIP.
P_2	Concentration of PIP_2.
P_3	Concentration of PIP_3.
B	Concentration of BtK.
v_4	Concentration of the complex $PIP_3 \cdot BtK^*$.
P_γ	Concentration of $PLC\gamma_2$.
v_5	Concentration of the complex $PLC\gamma_2 \cdot LAT_P$.
v_6	Concentration of the complex $PLC\gamma_2 \cdot LAT_{PP}$.
v_7	Concentration of the complex of phosphorylated $PLC\gamma_2$ ($PLC\gamma_{2P} \cdot LAT_P$).
v_8	Concentration of the complex of $PLC\gamma_{2P} \cdot LAT_{PP}$.
I	Concentration of IP_3.
D	Concentration of DAG.
I_{RC}	Concentration of IP_{3RC}.
v_9	Concentration of the complex of $IP_3 \cdot IP_{3RO}$.
Ca_1	Concentration of calcium in the dense tubular structure ($Ca^{(1)}$).
Ca_2	Concentration of calcium in the cytosol ($Ca^{(2)}$).

Integrating we find

$$L + L_P + L_{PP} + v_3 + v_5 + v_6 + v_7 + v_8 = \text{constant}$$

and applying the initial conditions we find

$$L + L_P + L_{PP} + v_3 + v_5 + v_6 + v_7 + v_8 = L_T$$

where
$$L_T = L_0 + L_{P0} + L_{PP0} + v_{30} + v_{50} + v_{60} + v_{70}. \qquad (2.47)$$

This means that LAT is conserved, using this we can reduce the number of parameters within the model and hence the number of equation we need to solve.

Similarly conservation of BtK (addition of equations (2.34) and (2.35)), the IP_3 receptors (addition of (2.43) and 2.44)), $PI3K$ (addition of (2.28) and (2.29)) and Ca^{2+} (addition of (2.45) and (2.46)) lead to,

$$B_T = B + v_4, \qquad (2.48)$$

$$I_T = I_{RC} + v_9, \qquad (2.49)$$

$$P_{KT} = P_K + v_3 \qquad (2.50)$$

and
$$Ca_T = Ca_1 + Ca_2. \qquad (2.51)$$

Substituting for L, v_4, P_K and Ca_1 into equations (2.26), (2.27), (2.29), (2.37)

– (2.40) and (2.46) leads to the following reduced system of equations.

$$\frac{dR_0^c}{dt} = -k_1 R_0^c C \tag{2.52}$$

$$\frac{dR_1^c}{dt} = k_1 R_0^c C - k_2 R_1^c \tag{2.53}$$

$$\frac{dR_2^c}{dt} = k_2 R_1^c - k_3 S R_2^c \tag{2.54}$$

$$\frac{dS}{dt} = -k_3 S R_2^c \tag{2.55}$$

$$\frac{dv_1}{dt} = k_3 S R_2^c - k_4 v_1 \tag{2.56}$$

$$\frac{dv_2}{dt} = k_4 v_1 - k_6 L_P v_2 \tag{2.57}$$

$$\frac{dL_P}{dt} = k_5 (L_T - L_P - L_P P - v_3 - v_5 - v_6 - v_7 - v_8) v_2$$
$$\qquad -k_6 L_P v_2 - k_{11} L_P P_\gamma \tag{2.58}$$

$$\frac{dL_{PP}}{dt} = k_6 L_P v_2 - k_7 L_{PP} (P_{KT} - v_3) - k_{12} L_{PP} P_\gamma \tag{2.59}$$

$$\frac{dv_3}{dt} = k_7 L_{PP} (P_{KT} - v_3) \tag{2.60}$$

$$\frac{dP}{dt} = -k_{17} P + k_{-17} P_1 + \frac{k_E}{k_s + P} \tag{2.61}$$

$$\frac{dP_1}{dt} = k_{17} P - k_{18} P_1 - k_{-17} P_1 + k_{-18} P_2 \tag{2.62}$$

$$\frac{dP_2}{dt} = -k_8 v_3 P_2 + k_9 P_3 P^{10} - k_{15} v_7 P_2$$
$$\qquad -k_{16} v_8 P_2 + k_{18} P - k_{-18} P_2 \tag{2.63}$$

$$\frac{dP_3}{dt} = k_8 v_3 P_2 - k_9 P_3 P^{10} - k_{10} P_3 B \tag{2.64}$$

$$\frac{dB}{dt} = -k_{10} P_3 B \tag{2.65}$$

$$\frac{dP_\gamma}{dt} = -k_{11} L_P P_\gamma - k_{12} L_{PP} P_\gamma \tag{2.66}$$

$$\frac{dv_5}{dt} = k_{11}L_P P_\gamma - k_{13}(B_T - B)v_5 \tag{2.67}$$

$$\frac{dv_6}{dt} = k_{12}L_{PP}P_\gamma - k_{14}(B_T - B)v_6 \tag{2.68}$$

$$\frac{dv_7}{dt} = k_{13}(B_T - B)v_5 \tag{2.69}$$

$$\frac{dv_8}{dt} = k_{14}(B_T - B)v_6 \tag{2.70}$$

$$\frac{dI}{dt} = k_{15}v_7 P_2 + k_{16}v_8 P_2 - k_{19}II_{RC} \tag{2.71}$$

$$\frac{dD}{dt} = k_{15}v_7 P_2 + k_{16}v_8 P_2 \tag{2.72}$$

$$\frac{dI_{RC}}{dt} = -k_{19}II_{RC} \tag{2.73}$$

$$\frac{dCa_2}{dt} = k_{20}(I_T - I_{RC})(Ca_T - Ca_2). \tag{2.74}$$

2.1 Parameterisation

After a literature search the initial conditions were supplied to us. Those concentrations which could not be found in the literature search were assumed to equal values of proteins who's values were known that played a similar role in the system. $PI3K$, BtK, $PLC\gamma_2$ and $PTEN$ are assumed to have the same concentration as SYK due to all these proteins being enzymes. LAT is assumed to have the same concentration as the receptors as it is an adaptor similar to these. We also assumed that all complexes start with zero concentration.

Reaction constants for which values could not be found were either assigned values of similar reaction constants or set relative to other parameters. k_5, k_6, $k_8 - k_{16}$, k_{19} and k_{20} are set relative to k_2, the parameter we will eventually non-dimensionalise with respect to. k_{-17} and k_{-18} are set relative to k_{17} and k_{18} so that the lipids PI, PIP and PIP_2 will stay constant in the absence of collagen.

Table 2.2: Values for Rate Constants

Parameter	Description	Value	Units	Reference
k_E	Source term for P	1×10^{-11}	$M^2 s^{-1}$	Assumed
k_s	Inhibition constant for source term	0.1	M	Assumed
k_1	Rate of free receptor/collagen binding.	8.62	$(Ms)^{-1}$	[8]
k_2	Rate at which bound receptor become active.	30	s^{-1}	[8]
k_3	Rate at which SYK·R$_2$ is formed.	325242	$(Ms)^{-1}$	[3]
k_4	Rate at which SYK$_P$·R$_2$ is formed.	200	s^{-1}	[3]
k_5	Rate of LAT phosphorylation.	2469	$(Ms)^{-1}$	Assumed
k_6	Rate of LAT$_P$ phosphorylation.	2469	$(Ms)^{-1}$	Assumed
k_7	Rate at which PI3K*·LAT$_{PP}$ is formed.	325242	$(Ms)^{-1}$	Assumed
k_8	Rate at which PIP$_3$ is formed.	60	$(Ms)^{-1}$	Assumed
k_9	Rate of PIP$_3$ converting to PIP$_2$.	60	$(Ms)^{-1}$	Assumed
k_{10}	Rate at which PIP$_3$·BtK* is formed.	60	$(Ms)^{-1}$	Assumed
k_{11}	Rate at which LAT$_P$·PLCγ2 is formed.	6000	$(Ms)^{-1}$	Assumed
k_{12}	Rate at which LAT$_{PP}$·PLCγ2 is formed.	6000	$(Ms)^{-1}$	Assumed
k_{13}	Rate at which PIP$_3$·BtK* phosphorylates LAT$_P$·PLCγ2.	15873	$(Ms)^{-1}$	Assumed
k_{14}	Rate at which PIP$_3$·BtK* phosphorylates LAT$_{PP}$·PLCγ2.	15873	$(Ms)^{-1}$	Assumed
k_{15}	Rate of IP$_3$ and DAG formation using LAT$_P$·PLCγ2P.	60	$(Ms)^{-1}$	Assumed
k_{16}	Rate of IP$_3$ and DAG formation using LAT$_{PP}$·PLCγ2P.	60	$(Ms)^{-1}$	Assumed
k_{17}	Rate at which PIP is formed from PI.	2.77	s^{-1}	[12]
k_{-17}	Rate at which PI is formed from PIP.	2.77	s^{-1}	Assumed
k_{18}	Rate at which PIP$_2$ is formed from PIP.	1.021	s^{-1}	[12]
k_{-18}	Rate at which PIP is formed from PIP$_2$.	1.021	s^{-1}	Assumed
k_{19}	Rate at which IP$_3$·IP$_{3RO}$ is produced.	60	$(Ms)^{-1}$	Assumed
k_{20}	Rate at which Ca$^{(2)}$ is produced.	6000	$(Ms)^{-1}$	Assumed

Table 2.3: Initial Data for concentrations

Parameter	Description	Value Used	Units	Reference
C	Collagen concentration.	9.5×10^{-4}	M	Experimental
R_{00}^c	Initial concentration of inactive, non-bound receptors.	2.96×10^{-8}	M	[13]
R_{10}^c	Initial concentration of inactive, bound receptors.	0	M	Assumed
R_{20}^c	Initial concentration of active, bound receptors.	0	M	Assumed
S_0	Initial concentration of SYK.	9.865×10^{-6}	M	[3]
v_{10}	Initial concentration of $SYK \cdot R_2$.	0	M	Assumed
v_{20}	Initial concentration of $SYK_P \cdot R_2$.	0	M	Assumed
L_0	Initial concentration of LAT.	2.96×10^{-8}	M	Assumed
L_{P0}	Initial concentration of LAT_P.	0	M	Assumed
L_{PP0}	Initial concentration of LAT_{PP}.	0	M	Assumed
P_{K0}	Initial concentration of PI3K.	9.865×10^{-6}	M	Assumed
v_{30}	Initial concentration of $PI3K^* \cdot LAT_{PP}$.	0	M	Assumed
P_0	Initial concentration of PI.	2.21×10^{-3}	M	[12]
P_{10}	Initial concentration of PIP.	3.69×10^{-4}	M	[12]
P_{20}	Initial concentration of PIP_2.	1.84×10^{-4}	M	[12]
P_{30}	Initial concentration of PIP_3.	0	M	Assumed
B_0	Initial concentration of BtK.	9.865×10^{-6}	M	Assumed
v_{40}	Initial concentration of $PIP_3 \cdot BtK^*$.	0	M	Assumed
$P_{\gamma 0}$	Initial concentration of $PLC\gamma_2$.	9.865×10^{-6}	M	Assumed
v_{50}	Initial concentration of $PLC\gamma_2 \cdot LAT_P$.	0	M	Assumed
v_{60}	Initial concentration of $PLC\gamma_2 \cdot LAT_{PP}$.	0	M	Assumed
v_{70}	Initial concentration of $PLC\gamma_{2P} \cdot LAT_P$.	0	M	Assumed
v_{80}	Initial concentration of $PLC\gamma_{2P} \cdot LAT_{PP}$.	0	M	Assumed
I_0	Initial concentration of IP_3.	0	M	Assumed
D_0	Initial concentration of DAG.	0	M	Assumed
I_{RC0}	Initial concentration of IP_{3RC}.	4.61×10^{-7}	M	[12]
v_{90}	Initial concentration of $IP_3 \cdot IP_{3RO}$.	0	M	Assumed
Ca_{10}	Initial concentration of Calcium in the DTS.	5×10^{-3}	M	[12]
Ca_{20}	Initial concentration of Calcium in the Cytosol.	50×10^{-9}	M	[12]
P_0^{10}	Initial concentration of PTEN.	9.865×10^{-6}	M	Assumed

2.2   Non–Dimensionalisation

Before solving our model we decided to non–dimensionalise the equations above. Non–dimensionalising removes the dimensions of the parameters so they can be directly compared and the reduces the number of parameters. We non–dimensional variable with respect to k_2 so

$$t = \frac{\tau}{k_2}, \tag{2.75}$$

where τ is the non-dimensional variable. We further more assume that all the concentrations are scaled with respect to Ca_T. So, for example

$$C = Ca_T \widehat{C}, \tag{2.76}$$

where $\widehat{C}$ is the non-dimensional concentration.

The system of equations then becomes

$$\frac{d\widehat{R_0^c}}{d\tau} = -\bar{k}_1 \widehat{R_0^c} \widehat{C} \tag{2.77}$$

$$\frac{d\widehat{R_1^c}}{d\tau} = \bar{k}_1 \widehat{R_0^c} \widehat{C} - \bar{k}_2 \widehat{R_1^c} \tag{2.78}$$

$$\frac{d\widehat{R_2^c}}{d\tau} = \bar{k}_2 \widehat{R_1^c} - \bar{k}_3 \widehat{S} \widehat{R_2^c} \tag{2.79}$$

$$\frac{d\widehat{S}}{d\tau} = -\bar{k}_3 \widehat{S} \widehat{R_2^c} \tag{2.80}$$

$$\frac{d\widehat{v_1}}{d\tau} = \bar{k}_3 \widehat{S} \widehat{R_2^c} - \bar{k}_4 \widehat{v_1} \tag{2.81}$$

$$\frac{d\widehat{v_2}}{d\tau} = \bar{k}_4 \widehat{v_1} - \bar{k}_6 \widehat{L_P} \widehat{v_2} \tag{2.82}$$

$$\frac{d\widehat{L_P}}{d\tau} = \bar{k}_5 (\widehat{L_T} - \widehat{L_P} - \widehat{L_{PP}} - \widehat{v_3} - \widehat{v_5} - \widehat{v_6} - \widehat{v_7} - \widehat{v_8}) \widehat{v_2}$$
$$- \bar{k}_6 \widehat{L_P} \widehat{v_2} - \bar{k}_{11} \widehat{L_P} \widehat{P_\gamma} \tag{2.83}$$

$$\frac{d\widehat{L_{PP}}}{d\tau} = \bar{k_6}\widehat{L_P}\widehat{v_2} - \bar{k_7}\widehat{L_{PP}}(\widehat{P_{KT}} - \widehat{v_3}) - \bar{k_{12}}\widehat{L_{PP}}\widehat{P_\gamma} \tag{2.84}$$

$$\frac{d\widehat{v_3}}{d\tau} = \bar{k_7}\widehat{L_{PP}}(\widehat{P_{KT}} - \widehat{v_3}) \tag{2.85}$$

$$\frac{d\widehat{P}}{d\tau} = -\bar{k_{17}}\widehat{P} + \bar{k_{-17}}\widehat{P_1} + \frac{\widehat{k_E}}{\bar{k_s} + \widehat{P}} \tag{2.86}$$

$$\frac{d\widehat{P_1}}{d\tau} = \bar{k_{17}}\widehat{P} - k_{18}\widehat{P_1} - \bar{k_{-17}}\widehat{P_1} + \bar{k_{-18}}\widehat{P_2} \tag{2.87}$$

$$\frac{d\widehat{P_2}}{d\tau} = -\bar{k_8}\widehat{v_3}\widehat{P_2} + \bar{k_9}\widehat{P_3}\widehat{P^{10}} - \bar{k_{15}}\widehat{v_7}\widehat{P_2} - \bar{k_{16}}\widehat{v_8}\widehat{P_2}$$
$$+\bar{k_{18}}\widehat{P} - \bar{k_{-18}}\widehat{P_2} \tag{2.88}$$

$$\frac{d\widehat{P_3}}{d\tau} = \bar{k_8}\widehat{v_3}\widehat{P_2} - \bar{k_9}\widehat{P_3}\widehat{P^{10}} - \bar{k_{10}}\widehat{P_3}\widehat{B} \tag{2.89}$$

$$\frac{d\widehat{B}}{d\tau} = -\bar{k_{10}}\widehat{P_3}\widehat{B} \tag{2.90}$$

$$\frac{d\widehat{P_\gamma}}{d\tau} = -\bar{k_{11}}\widehat{L_P}\widehat{P_\gamma} - \bar{k_{12}}\widehat{L_{PP}}\widehat{P_\gamma} \tag{2.91}$$

$$\frac{d\widehat{v_5}}{d\tau} = \bar{k_{11}}\widehat{L_P}\widehat{P_\gamma} - \bar{k_{13}}(\widehat{B_T} - \widehat{B})\widehat{v_5} \tag{2.92}$$

$$\frac{d\widehat{v_6}}{d\tau} = \bar{k_{12}}\widehat{L_{PP}}\widehat{P_\gamma} - \bar{k_{14}}(\widehat{B_T} - \widehat{B})\widehat{v_6} \tag{2.93}$$

$$\frac{d\widehat{v_7}}{d\tau} = \bar{k_{13}}(\widehat{B_T} - \widehat{B})\widehat{v_5} \tag{2.94}$$

$$\frac{d\widehat{v_8}}{d\tau} = \bar{k_{14}}(\widehat{B_T} - \widehat{B})\widehat{v_6} \tag{2.95}$$

$$\frac{d\widehat{I}}{d\tau} = \bar{k_{15}}\widehat{v_7}\widehat{P_2} + \bar{k_{16}}\widehat{v_8}\widehat{P_2} - \bar{k_{19}}\widehat{I}\widehat{I_{RC}} \tag{2.96}$$

$$\frac{d\widehat{D}}{d\tau} = \bar{k_{15}}\widehat{v_7}\widehat{P_2} + \bar{k_{16}}\widehat{v_8}\widehat{P_2} \tag{2.97}$$

$$\frac{d\widehat{I_{RC}}}{d\tau} = -\bar{k_{19}}\widehat{I}\widehat{I_{RC}} \tag{2.98}$$

$$\frac{d\widehat{Ca_2}}{d\tau} = \bar{k_{20}}(\widehat{I_T} - \widehat{I_{RC}})(\widehat{Ca_T} - \widehat{Ca_2}). \tag{2.99}$$

where

$$\bar{k}_E = \frac{k_E}{k_2 Ca_T^2}, \ \bar{k}_s = \frac{k_s}{Ca_T}, \tag{2.100}$$

$$\bar{k}_1 = \frac{k_1 Ca_T}{k_2}, \ \bar{k}_3 = \frac{k_3 Ca_T}{k_2}, \ \bar{k}_4 = \frac{k_4}{k_2}, \tag{2.101}$$

$$\bar{k}_5 = \frac{k_5 Ca_T}{k_2}, \ \bar{k}_6 = \frac{k_6 Ca_T}{k_2}, \ \bar{k}_7 = \frac{k_7 Ca_T}{k_2}, \ \bar{k}_8 = \frac{k_8 Ca_T}{k_2}, \tag{2.102}$$

$$\bar{k}_9 = \frac{k_9 Ca_T}{k_2}, \ \bar{k}_{10} = \frac{k_{10} Ca_T}{k_2}, \ \bar{k}_{11} = \frac{k_{11} Ca_T}{k_2}, \ \bar{k}_{12} = \frac{k_{12} Ca_T}{k_2}, \tag{2.103}$$

$$\bar{k}_{13} = \frac{k_{13} Ca_T}{k_2}, \ \bar{k}_{14} = \frac{k_{14} Ca_T}{k_2}, \ \bar{k}_{15} = \frac{k_{15} Ca_T}{k_2}, \ \bar{k}_{16} = \frac{k_{10} Ca_T}{k_2}, \tag{2.104}$$

$$\bar{k}_{17} = \frac{k_{17}}{k_2}, \ \bar{k}_{-17} = \frac{k_{-17}}{k_2}, \ \bar{k}_{18} = \frac{k_{18}}{k_2}, \ \bar{k}_{-18} = \frac{k_{-18}}{k_2}, \tag{2.105}$$

$$\bar{k}_{19} = \frac{k_{19} Ca_T}{k_2} \text{ and } \bar{k}_{20} = \frac{k_{20} Ca_T}{k_2} \tag{2.106}$$

The values of these non–dimensional parameters are in table 2.2 with the non–dimensionalised initial conditions as in table 2.2.

2.3   Solving the System

The large variation in scales of the parameters in the system of differential equations makes this a stiff system. According to [7], a stiff system is one which given

$$y'(t) = f'(y(t))$$

has the property that $f'(y)$ is much greater than (in absolute value or norm) than $y'(t)$. This means that most numerical methods are unstable unless the step size is extremely small which becomes numerically costly. Because of this, special methods such as backwards differentiation must be employed. This section gives a basic outline to this method, as we use a set MATLAB solver we do not need to implement this method ourselves. For greater detail

Parameter	Description	Value
$\bar{k}_E$	Source term for PI	1.3×10^{-6}
$\bar{k}_s$	Inhibition constant for source term	20
$\bar{k}_1$	Rate of free receptor/collagen binding.	0.0014
$\bar{k}_2$	Rate at which bound receptor become active.	1
$\bar{k}_3$	Rate at which SYK·R$_2$ is formed.	54.21
$\bar{k}_4$	Rate at which SYK$_P$·R$_2$ is formed.	6.67
$\bar{k}_5$	Rate of LAT phosphorylation.	0.41
$\bar{k}_6$	Rate of LAT$_P$ phosphorylation.	0.41
$\bar{k}_7$	Rate at which PI3K*·LAT$_{PP}$ is formed.	54.21
$\bar{k}_8$	Rate at which PIP$_3$ is formed.	0.01
$\bar{k}_9$	Rate of PIP$_3$ converting to PIP$_2$.	0.01
$\bar{k}_{10}$	Rate at which PIP$_3$·BtK* is formed.	0.01
$\bar{k}_{11}$	Rate at which LAT$_P$·PLCγ_2 is formed.	1
$\bar{k}_{12}$	Rate at which LAT$_{PP}$·PLCγ_2 is formed.	1
$\bar{k}_{13}$	Rate at which PIP$_3$·BtK* phosphorylates LAT$_P$·PLCγ_2.	2.65
$\bar{k}_{14}$	Rate at which PIP$_3$·BtK* phosphorylates LAT$_{PP}$·PLCγ_2.	2.65
$\bar{k}_{15}$	Rate of IP$_3$ and DAG formation using LAT$_P$·PLCγ_{2P}.	0.01
$\bar{k}_{16}$	Rate of IP$_3$ and DAG formation using LAT$_{PP}$·PLCγ_{2P}.	0.01
$\bar{k}_{17}$	Rate at which PIP is formed from PI.	0.092
$\bar{k}_{-17}$	Rate at which PI is formed from PIP.	0.092
$\bar{k}_{18}$	Rate at which PIP$_2$ is formed from PIP.	0.034
$\bar{k}_{-18}$	Rate at which PIP is formed from PIP$_2$.	0.0340
$\bar{k}_{19}$	Rate at which IP$_3$:IP$_{3RO}$ is produced.	0.01
$\bar{k}_{20}$	Rate at which Ca$^{(2)}$ is produced.	1

Parameter	Description	Value
$\widehat{C}$	Collagen concentration.	0.19
$\widehat{R^c_{00}}$	Initial concentration of inactive, non-bound receptors.	5.92×10^{-6}
$\widehat{R^c_{10}}$	Initial concentration of inactive, bound receptors.	0
$\widehat{R^c_{20}}$	Initial concentration of active, bound receptors.	0
$\widehat{S_0}$	Initial concentration of SYK.	0.002
$\widehat{v_{10}}$	Initial concentration of $SYK \cdot R_2$.	0
$\widehat{v_{20}}$	Initial concentration of $SYK_P \cdot R_2$.	0
$\widehat{L_0}$	Initial concentration of LAT.	5.92×10^{-6}
$\widehat{L_{P0}}$	Initial concentration of LAT_P.	0
$\widehat{L_{PP0}}$	Initial concentration of LAT_{PP}.	0
$\widehat{P_{K0}}$	Initial concentration of PI3K.	0.002
$\widehat{v_{30}}$	Initial concentration of $PI3K^* \cdot LAT_{PP}$.	0
$\widehat{P_0}$	Initial concentration of PI.	0.44
$\widehat{P_{10}}$	Initial concentration of PIP.	0.074
$\widehat{P_{20}}$	Initial concentration of PIP_2.	0.037
$\widehat{P_{30}}$	Initial concentration of PIP_3.	0
$\widehat{B_0}$	Initial concentration of BtK.	1.97×10^{-5}
$\widehat{v_{40}}$	Initial concentration of $PIP_3 \cdot BtK^*$.	0
$\widehat{P_{\gamma 0}}$	Initial concentration of $PLC\gamma_2$.	1.97×10^{-5}
$\widehat{v_{50}}$	Initial concentration of $PLC\gamma_2 \cdot LAT_P$.	0
$\widehat{v_{60}}$	Initial concentration of $PLC\gamma_2 \cdot LAT_{PP}$.	0
$\widehat{v_{70}}$	Initial concentration of $PLC\gamma_{2P} \cdot LAT_P$.	0
$\widehat{v_{80}}$	Initial concentration of $PLC\gamma_{2P} \cdot LAT_{PP}$.	0
$\widehat{I_0}$	Initial concentration of IP_3.	0
$\widehat{D_0}$	Initial concentration of DAG.	0
$\widehat{I_{RC0}}$	Initial concentration of IP_{3RC}.	0
$\widehat{v_{90}}$	Initial concentration of $IP_3 \cdot IP_{3RO}$.	0
$\widehat{Ca_{10}}$	Initial concentration of Calcium in the Dense Tubular Structure.	1
$\widehat{Ca_{20}}$	Initial concentration of Calcium in the Cytosol.	1×10^{-5}
$\widehat{P^{10}_0}$	Initial concentration of PTEN.	1.97×10^{-5}

refer to [7].

2.3.1 Backwards Differentiation

The backward differentiation formula are a set of implicit methods that can be used to numerically solve differential equations. They are linear multistep methods that approximate the derivative of the function using data that has been calculated at previous timesteps.

The general form of a linear multistep method to solve the differential equation

$$\underline{y}' = \underline{f}(t, \underline{y}), \ \underline{y}(t_0) = y_0$$

is

$$\sum_{i=0}^{k} a_i \underline{y}_{n-i} = h \sum_{i=0}^{k} b_i \underline{f}_{n-i}.$$

Backwards differentiation methods have $b_i = 0$ for $i > 0$ and so the general formula becomes

$$\sum_{i=0}^{k} a_i \underline{y}_{n-i} = h b_0 \underline{f}_n.$$

By having $b_i = 0$ for $i > 0$ backwards differentiation methods have the point at infinity on the interior of their stability region making them useful for solving stiff systems. As backwards differentiation is an implicit method, non-linear equations must be solved. This is normally done by using a solver such as Newton's Method.

We used the MATLAB solver ode15s to solve our system of differential equations, as this solver can optionally use backwards differentiation with variable order.
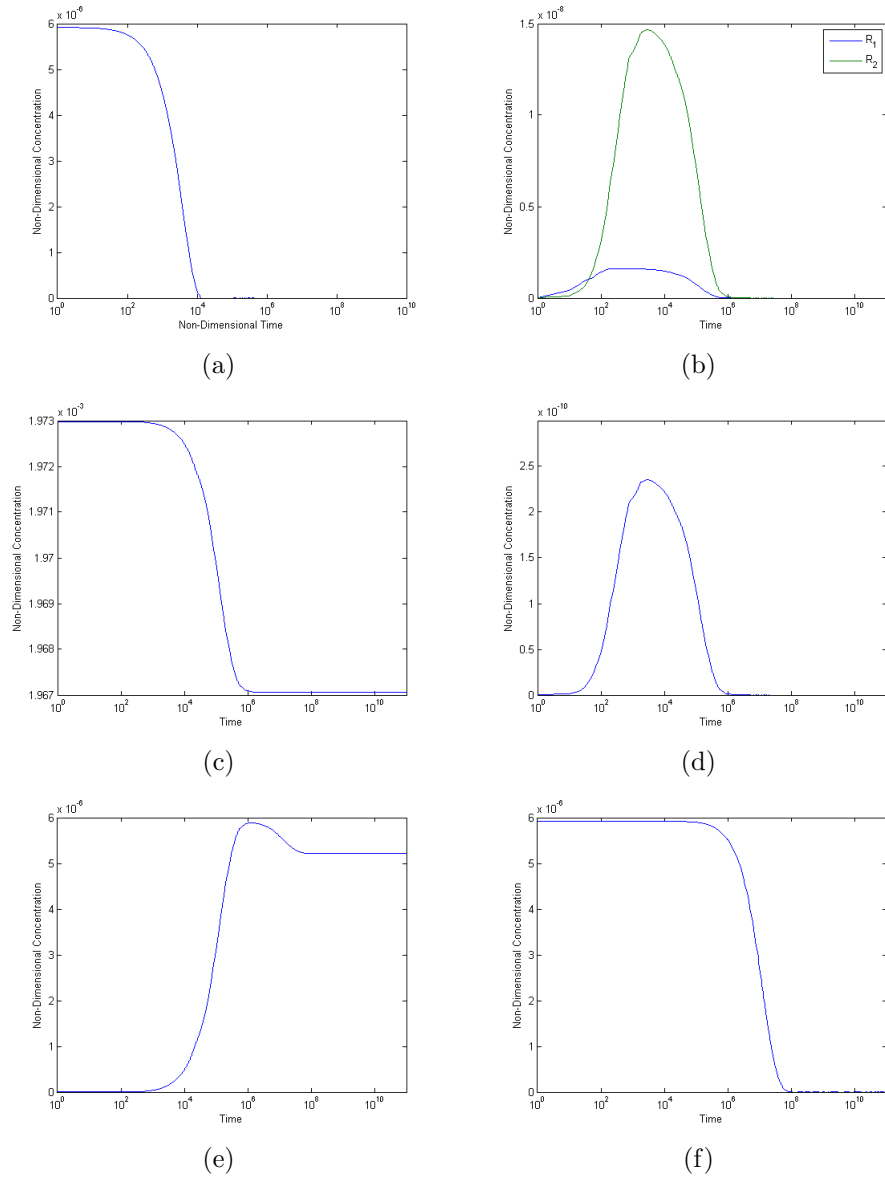
Figure 2.3: Graphs of Non–Dimensional Concentration against Time in seconds. (a)R_0, (b)R_1 and R_2, (c)SYK, (d)$SYK \cdot R_2$, (e)$SYK_P \cdot R_2$ and (f)LAT.
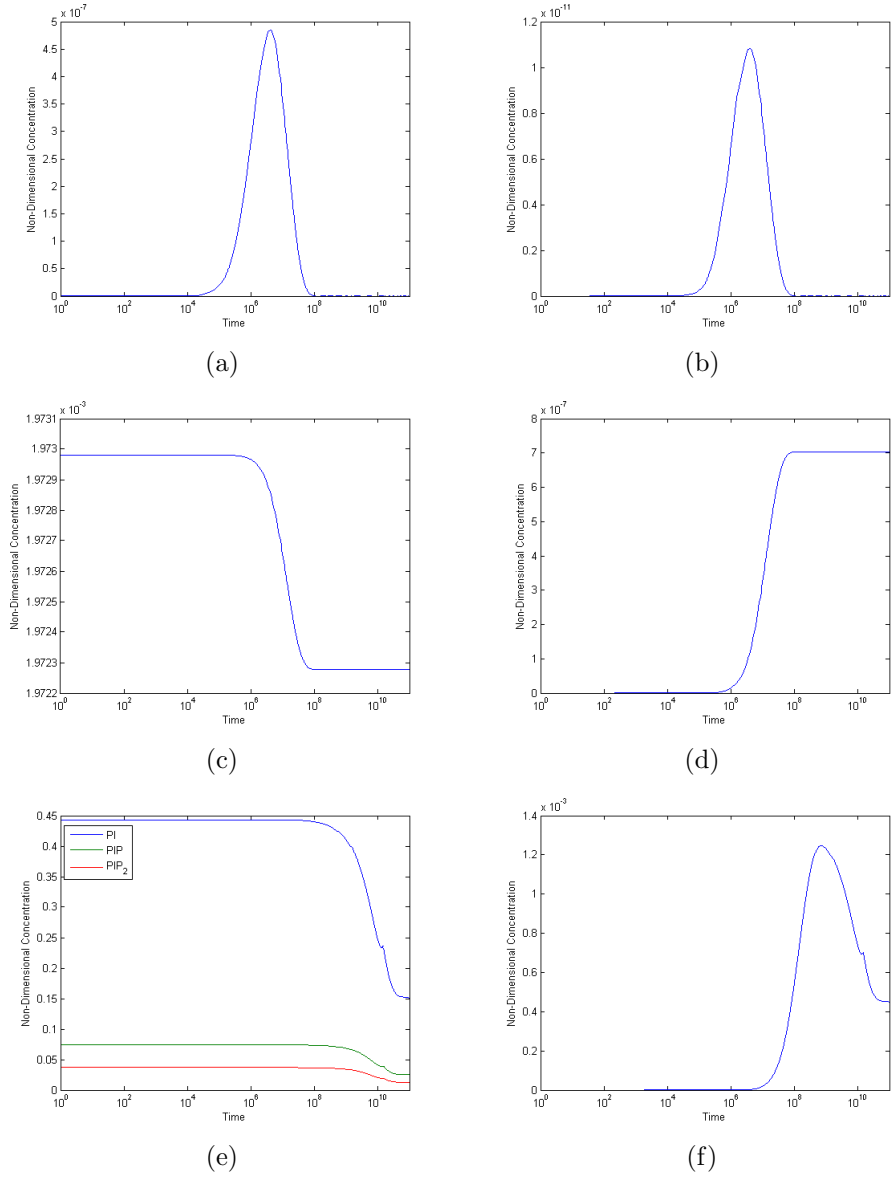
Figure 2.4: Graphs of Non–Dimensional Concentration against Time in seconds. (a)LAT_P, (b)LAT_{PP}, (c)$PI3K$, (d)$PI3K^* \cdot LAT_{PP}$, (e)PI, PIP and PIP_2 and (f)PIP_3.
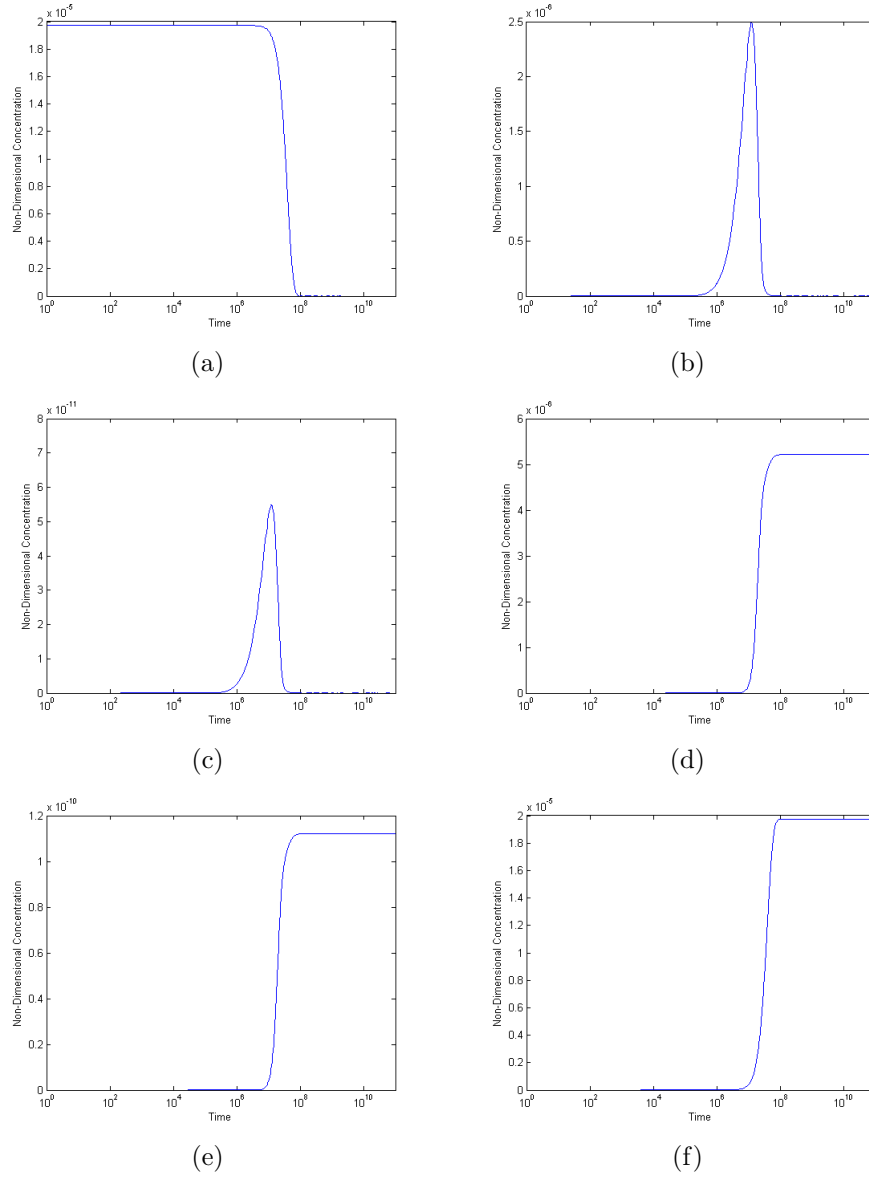
Figure 2.5: Graphs of Non–Dimensional Concentration against Time in seconds. (a)BtK, (b)$LAT_P \cdot PLC\gamma_2$, (c)$LAT_{PP} \cdot PLC\gamma_2$, (d)$LAT_P \cdot PLC\gamma_{2P}$, (e)$LAT_{PP} \cdot PLC\gamma_{2P}$ and (f)$PIP_3 \cdot BtK^*$.
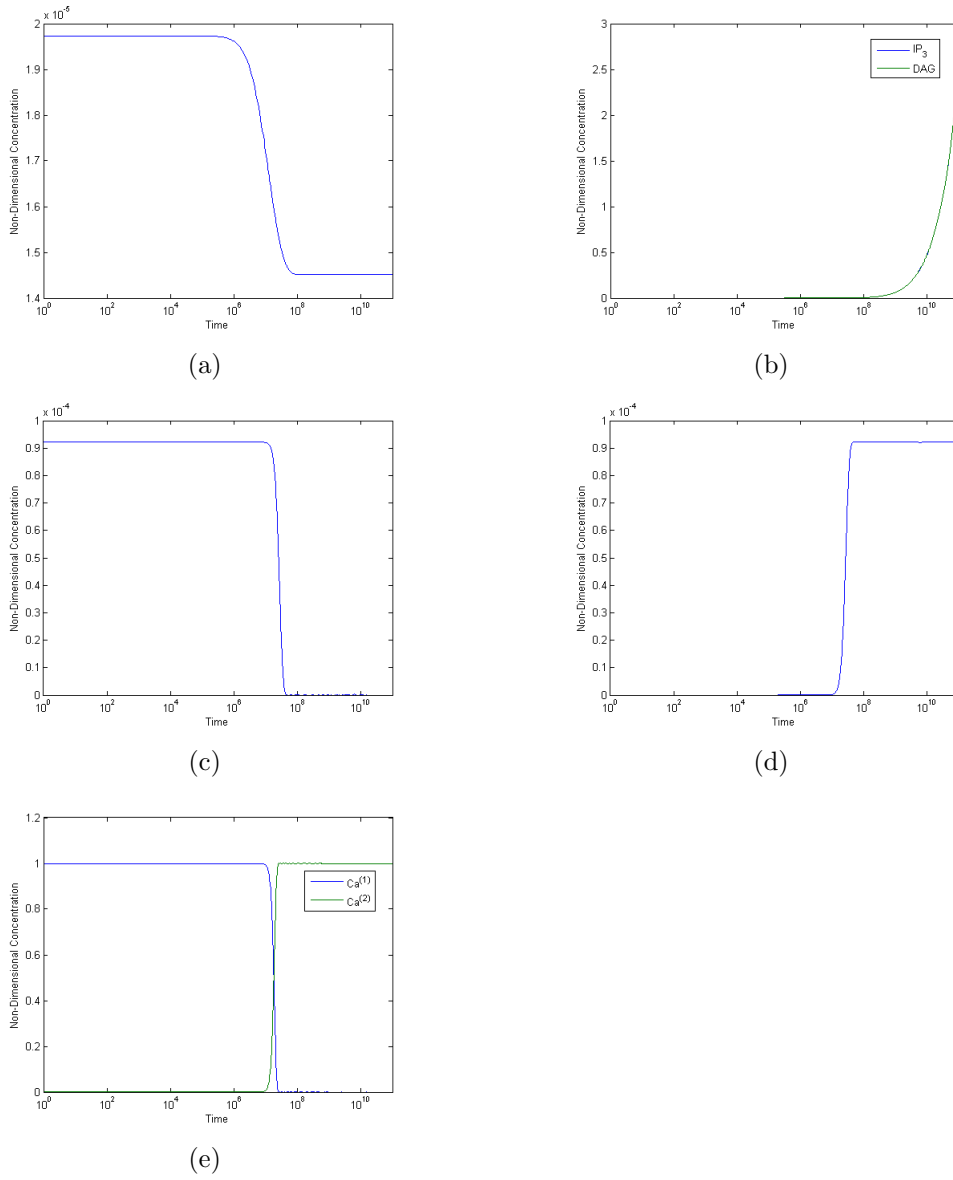
Figure 2.6: Graphs of Non–Dimensional Concentration against Time in seconds. (a)$PLC\gamma_2$, (b)IP_3 and DAG, (c)IP_{3RC}, (d)$IP_3 \cdot IP_{3RO}$, (e)$Ca^{(1)}$ and $Ca^{(2)}$.

2.4   Model Solutions

Figures (2.3) – (2.6) are the numerical solution to the system of differential equations described in the previous section. They show the change in concentration of the proteins involved in the pathway described in Figure (2.2). Figure (2.3) shows the concentrations of proteins at the beginning of the pathway . We can see how quickly the collagen binds to the receptor and the receptors become active, this is due to collagen being in excess. SYK then binds with these active receptors, reducing it's concentration, and auto-phosphorylates. This phosphorylated complex then is used in the auto–phosphorylation of LAT, producing LAT_P and being used up when generating LAT_{PP}.

In Figure (2.4) we see LAT_{PP} being used to activate $PI3K$ by forming the complex $LAT_{PP} \cdot PI3K$. The lipids PI, PIP and PIP_2 slowly arrive at a steady state with PIP_3 rising as it's generated then reducing as the reaction with BtK becomes more dominant. We can see in Figure (2.5) that BtK reduces as soon as PIP_3 is generated.

Also in Figure (2.5) we find that qualitatively the graphs for $LAT_P \cdot PLC\gamma_2$ and $LAT_{PP} \cdot PLC\gamma_2$ as well as $LAT_P \cdot PLC\gamma_{2P}$ and $LAT_{PP} \cdot PLC\gamma_{2P}$ show the same behaviour. This is due to the reaction constants for generation and loss of these proteins being equivalent.

Figure (2.6) shows that IP_3 and DAG do not reach a steady state. This is due to the differential equation for DAG, equation (2.72), containing only positive terms that remain non-zero and the one negative term in equation (2.96) tending to zero with the other terms remaining non-zero. We can also see our model correctly predicts the transferrence of calcium from the DTS to the cytosol as required.

There is a wide variation in the changes in concentration of the proteins. For example the peak in R_1 and R_2 is small due to the excess collagen quickly

driving the reaction (2.1) and (2.2) combined with the fast reaction rates in reaction (2.3). This means that R_1 and R_2 are used almost as fast as they are generated. Similarly, this is the case for only small increases LAT_P, LAT_{PP} and $LAT_{PP} \cdot PLC\gamma_2$ before their reduction. $PI3K^* \cdot LAT_{PP}$ and $LAT_{PP} \cdot PLC\gamma_2$ settle to small concentration, this is due to LAT, of one form or another being involved in many of the reactions and so the initial concentration of LAT being split.

2.5 Sensitivity Analysis of the Model

Sensitivity analysis is a way to see whether the output of the model is sensitive to any changes in the parameters. It is important to know which parameters have the most affect on the outcome of the model so we know which reactions or chemicals to target in the case of platelet diseases.

2.5.1 Methods of Sensitivity analysis

There are two different types of sensitivity analysis, *local* and *global*. Local sensitivity analysis focuses on the contribution of a single parameter to the overall model while global analysis looks at the changes of parameters in relation to each other and the effect these relations have on the model. We will be looking at local sensitivity analysis as it is more relevent to our model.

There are many different ways to perform a sensitivity analysis. Ihekwaba et al. [6] used the formula

$$S_P^M = \frac{\delta M/M}{\delta P/P}$$

where P is the parameter that is varied, M is the response of the overall system and δM is the incremental change in the response due to the incremental change in the parameter δP to find sensitivity coefficients. They individually

varied each parameter and used several features of the results (first, second and third oscillations) of their model to quantify the effect on the outcome.

We, however, do not have enough features on our graphs to make this method work effectively. So the method which we will use to analyse our model, is to vary each parameter in the model individually and then merely look at the effect on one key feature of the model. We times each parameter by 10, 50, 100, 0.1, 0.05 and 0.01 while keeping the rest at their original value. We measure the time it took for Ca_2 to be higher that Ca_1 and compare it to the model with original values.

2.5.2   Analysis and Discussion

Unfortunately numerical problems meant we could not run a sensitivity analysis for IP_3 or BtK initial concentration. However all other non-zero concentrations were taken into account.

Looking at figure (2.7) we can see that changes in k_{20} have a large affect on the output. This is expected as k_{20} is the rate of transfer between calcium in the DTS and cytosol. Similarly the affect of k_{19} could be predicted as it opens the ion channel so transferrence can take place. The rate constants k_{17}, k_{-17}, k_{18} and k_{-18} which control lipid cycling can also be seen to be important. This could be as PIP_2 is needed to generate IP_3, so the more PIP_2 in the system the more IP_3 is produced, which is needed to release calcium from the DTS. The need for IP_3 in the system is also backed up by the affect of varying k_{15}. It is possible that a greater amount of IP_3 is produced from $LAT_P \cdot PLC\gamma_{2P}$ than from $LAT_{PP} \cdot PLC\gamma_{2P}$ which is why it has more of an affect on the output. It can be seen reduction in k_5 lengthens the time it takes for calcium to be released. From Figure (2.2) we see that the model branches into two after LAT_P is produced, k_5 is at the junction of this branching and so has a greater affect on the model output as LAT_P avaliability will contribute to many reaction downstream indirectly.
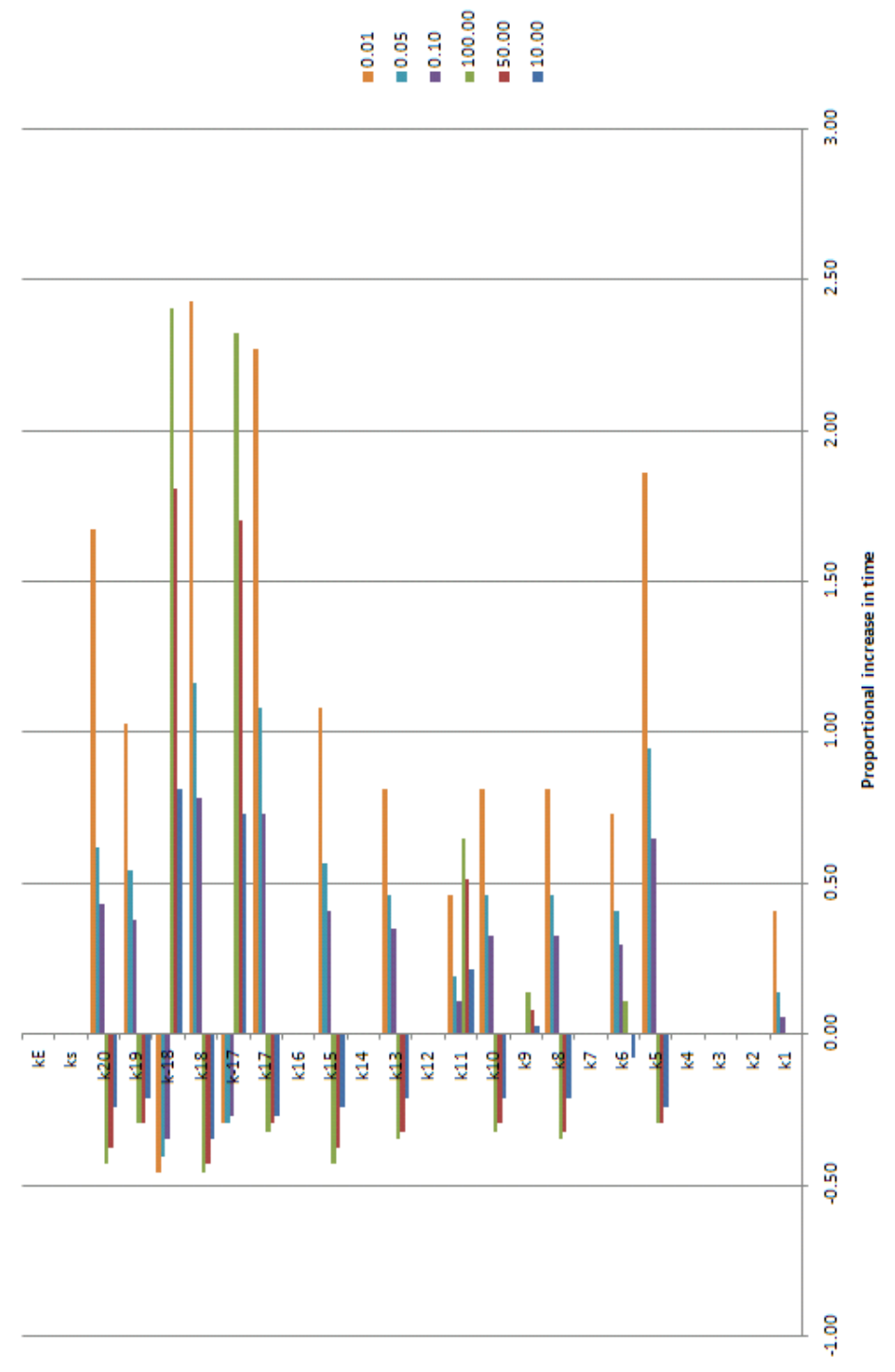
Figure 2.7: Graph showing affect of changing rate constants on model output
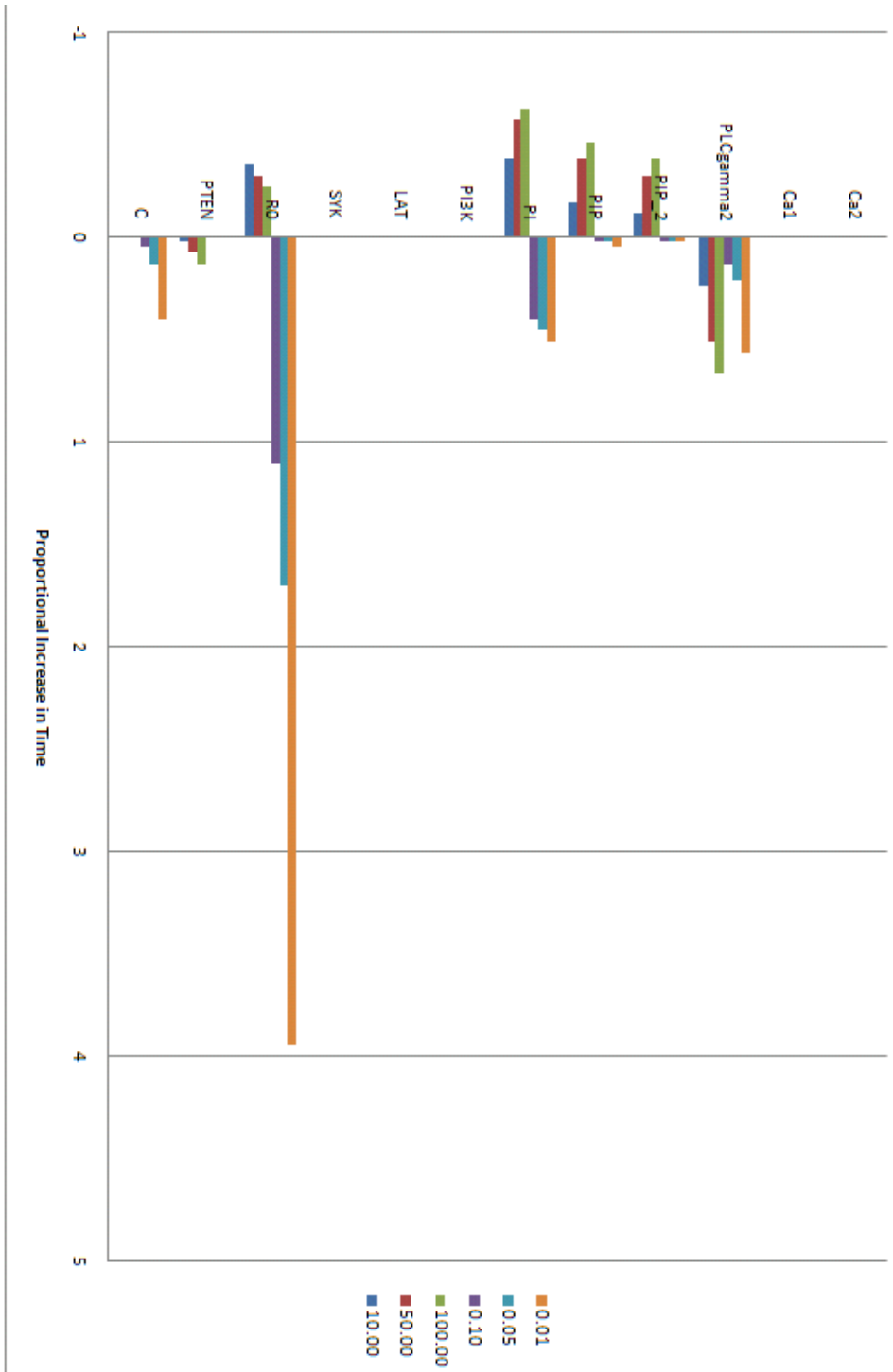
Figure 2.8: Graph showing affect of changing initial concentrations on model output

The next most influential rates are k_6, k_8, k_{10} and k_{13}. The first three of these rates lie on the same branch of the model. It is this branch eventually generates $PIP_3 \cdot BtK^*$, which is necessary to produce $LAT_P \cdot PLC\gamma_{2P}$ and $LAT_{PP} \cdot PLC\gamma_{2P}$ which are needed for IP_3 generation. k_{13} is the rate that controls the formation of $LAT_P \cdot PLC\gamma_{2P}$, which preceeds the reaction which k_{15} controls, so is influential for a similar reason. An increase or decrease in k_{11} increases the time it takes for the transfer of calcium. This could be because it regulates the rate at which LAT_P is used to form $LAT_P \cdot PLC\gamma_2$. A decrease in this parameter would mean that $LAT_P \cdot PLC\gamma_2$, which is needed to form $LAT_P \cdot PLC\gamma_{2P}$ and eventually IP_3 production, is formed at a slower rate. Yet an increase in this parameter would take LAT_P away from the other half of the model which produces $PIP_3 \cdot BtK^*$, which is also vital for eventual IP_3 production. We could also have predicted that k_1 would have an affect as it controls how quickly the model starts.

It can be seen that changes in k_2, k_3 and k_4 have no affect on the model. This could be due to other reactions taking place at a much slower rate later on and so the speed of these early reaction do not have a marked affect on the system. A similar remark could be made about k_7. As it is among the fastest rates any change is compensated by the slower rates downstream. k_{12}, k_{14} and k_{16} are on the same branch of the model. This is the branch that, as previously stated, may produce less IP_3 which may account for their lack of influence.

We find that only changes in seven of the initial concentrations has any affect on the outcome of the model. The lipids PI, PIP and PIP_2 have an affect for the same reason as the reaction constants controlling this cycle do. Changes in R_0 make a large difference. This is due to the more receptors there are the faster the model will initiate. Reductions in the amount of collagen stops it from being in excess and so not all the receptors will activate, slowing the time it takes for the desired output. Increasing $PTEN$ increases the amount of PIP_3 being turned back into PIP_2 and so slows the

time. $PLC\gamma_2$ slows the time it takes for calcium transfer if it is increased or decreased. This could be because if the concentration is high, it reacts with more LAT_{PP} taking it away from the branch which produces $PIP_3 \cdot BtK^*$ which is important as stated before. If there is low concentration not enough $LAT_P \cdot PLC\gamma_2$ will be produced on the branch that produces the greater amount of IP_3.

Chapter 3

Improving the Model

Although the model transfers calcium from the DTS to the cytosol as required, however there are some problems. The fact that IP_3 and DAG never reach a steady state, and that the DTS empties of calcium completely is intuitively wrong. Now we try and adapt the model to make it more realistic. We add the recycling of IP_3 and DAG aswell of the recycling of calcium in the cytosol to the DTS. Changes to our model can be seen in Figure (3.1). We add the following two reaction equations,

$$IP_3 + DAG \overset{k_{21}}{\rightarrow} PI \tag{3.1}$$

$$Ca^{(2)} + SERCA \overset{k_{22}}{\rightarrow} Ca^{(1)} + SERCA \tag{3.2}$$

and so equations (2.61), (2.71), (2.72) and (2.74) now become

$$\frac{dP}{dt} = -k_{17}P + k_{-17}P_1 + k_{21}DI \tag{3.3}$$

$$\frac{dI}{dt} = k_{15}v_7P_2 + k_{16}v_8P_2 - k_{19}II_{RC} - k_{21}DI \tag{3.4}$$

$$\tag{3.5}$$
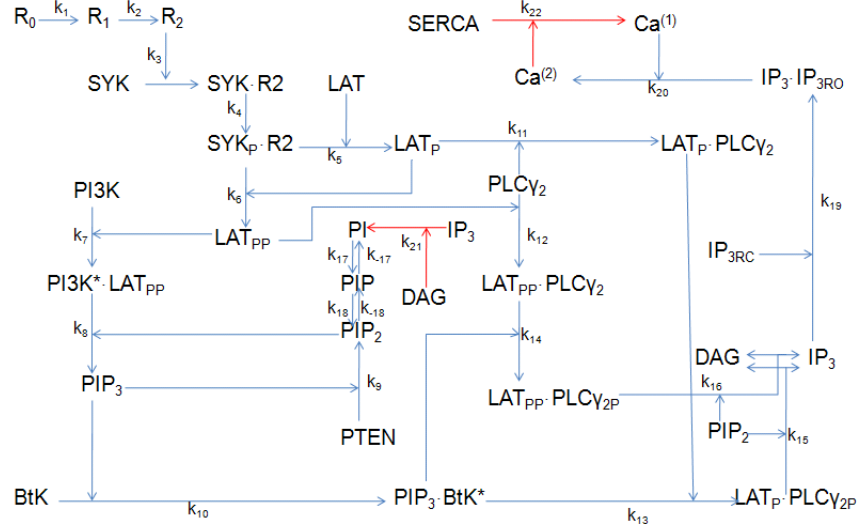
Figure 3.1: Schematic Diagram of improved Model. Changes are shown in red.

$$\frac{dD}{dt} = k_{15}v_7P_2 + k_{16}v_8P_2 - k_{21}DI \tag{3.6}$$

$$\frac{dCa_2}{dt} = k_{20}(I_T - I_{RC})(Ca_T - Ca_2) - k_{22}Ca_2S^A. \tag{3.7}$$

and we assume the initial concentration of $SERCA$ to be $S_0^A = 9.865 \times 10^{-6}M$, the same as P^{10}. We also assume $k_{21} = 553.79(Ms)^{-1}$ and $k_{22} = 5999.94(Ms)^{-1}$ set with respect to k_{17} and k_2 respectively.

Non-Dimensionalising with

$$t = \frac{k_2}{\tau}$$

as before leads to these equations becoming

$$\frac{d\widehat{P}}{d\tau} = -\bar{k_{17}}\widehat{P} + \bar{k_{-17}}\widehat{P_1} + \bar{k_{21}}\widehat{D}\widehat{I} \tag{3.8}$$

$$\frac{d\widehat{I}}{d\tau} = \bar{k_{15}}\widehat{v_7}\widehat{P_2} + \bar{k_{16}}\widehat{v_8}\widehat{P_2} - \bar{k_{19}}\widehat{I}\widehat{I_{RC}} - \bar{k_{21}}\widehat{D}\widehat{I} \qquad (3.9)$$

$$\frac{d\widehat{D}}{d\tau} = \bar{k_{15}}\widehat{v_7}\widehat{P_2} + \bar{k_{16}}\widehat{v_8}\widehat{P_2} - \bar{k_{21}}\widehat{D}\widehat{I} \qquad (3.10)$$

$$\frac{d\widehat{Ca_2}}{d\tau} = \bar{k_{20}}(\widehat{I_T} - \widehat{I_{RC}})(\widehat{Ca_T} - \widehat{Ca_2}) - \bar{k_{22}}\widehat{Ca_2}\widehat{S^A} \qquad (3.11)$$

with

$$\bar{k_{21}} = \frac{k_{21}Ca_T}{k_2}, \quad \bar{k_{22}} = \frac{k_{22}Ca_T}{k_2}$$

and the other non-dimensional parameters as before. Hence we have $\widehat{S_0^A} = 1.97 \times 10^{-5}$, $\bar{k_{21}} = 0.092$ and $\bar{k_{22}} = 1$.

3.1 Model Solutions

For the most part there is little difference between the behaviour of our improved model to the first. The main differences can be seen in Figure (3.2). IP_3 and DAG now reach a steady state and the DTS does not empty of calcium, which is what we required. It may also be noticed that the lipids PI, PIP, PIP_2 and PIP_3 reach a steady state much sooner, in fact they differ little from their original values. This is due to the recycling of DAG and IP_3 balancing with PIP_2 being used. PIP_3 now rises to its steady state, as opposed to rising then falling like before. This is due to PIP_2 maintaining a higher concentration.

3.2 Sensitivity Analysis

The sensitivity analysis of the improved model was carried out in the same way as in the previous section. Figures (3.3) and (3.5) show the results of this analysis. Figure (3.4) show the results for changing rate constants without
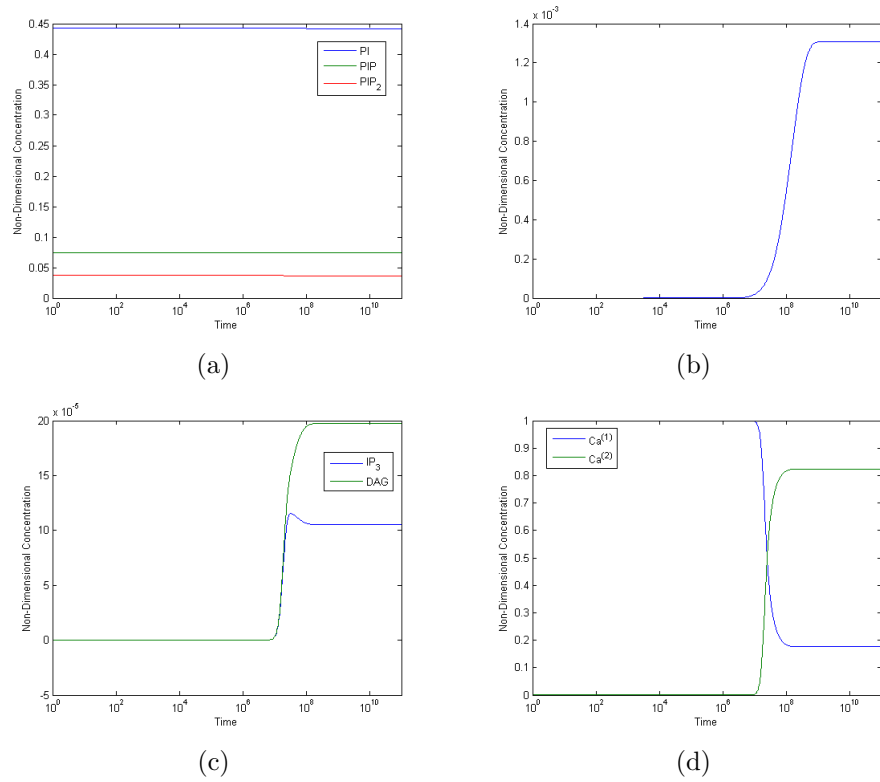
Figure 3.2: Graphs for the Improved Model. (a)PI, PIP and PIP_2, (b) PIP_3, (c) IP_3 and DAG (d) $Ca^{(1)}$ and $Ca^{(2)}$.

k_{19} to give a better idea of scale.

For the most part the same parameters and concentrations affect the model output for similar reasons as before. Differences in the parameters affecting the models include k_{20} having less affect in our improved model. This is due to the recycling in this model. Also k_{22} and $SERCA$ have an affect on the output. This is due to higher $SERCA$ concentration, or faster rate constant, meaning more calcium gets moved back into the DTS.

It may also be noted that the model output is generally more sensitive to changes in parameters that our previous model. This could be due to the fact that IP_3 and DAG now feed back into the lipid cycle. This means that parameters that previously wouldn't have affected this cycle now do, and as already noted changes in the lipid cycle have a great affect in the model.

3.3 Check of the Model

To check the model we test it under the condition where no collagen is present. We find that there is no movement of the proteins from their initial conditions.

3.4 Steady State Analysis

Steady state analysis will tell us how the concentrations behave when a steady state is reached. To do this analysis, we set the left hand side or our system of differential equations to zero. Doing this and substituting leaves us with
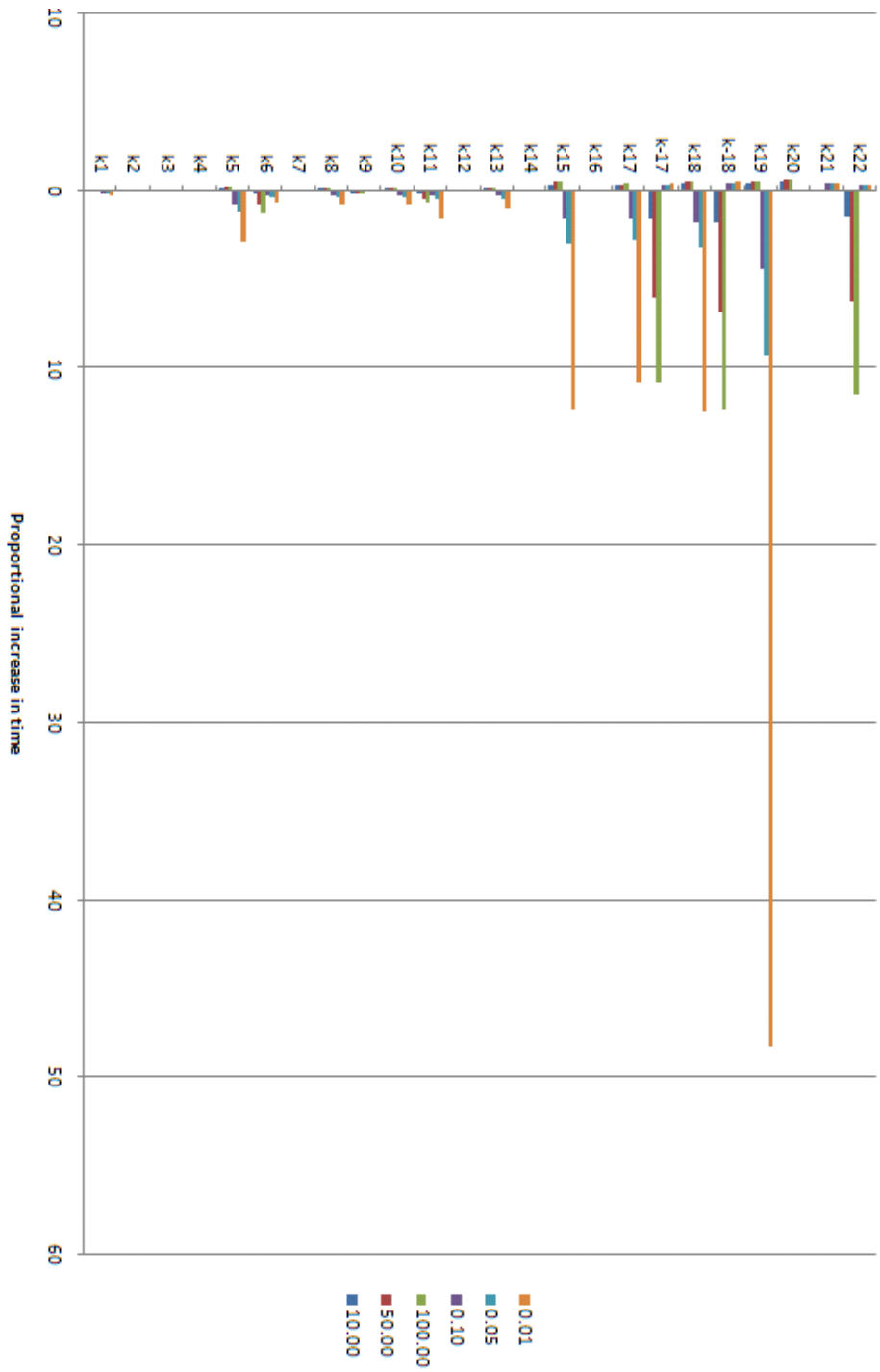
Figure 3.3: Graph showing affect of changing rate constants on model output
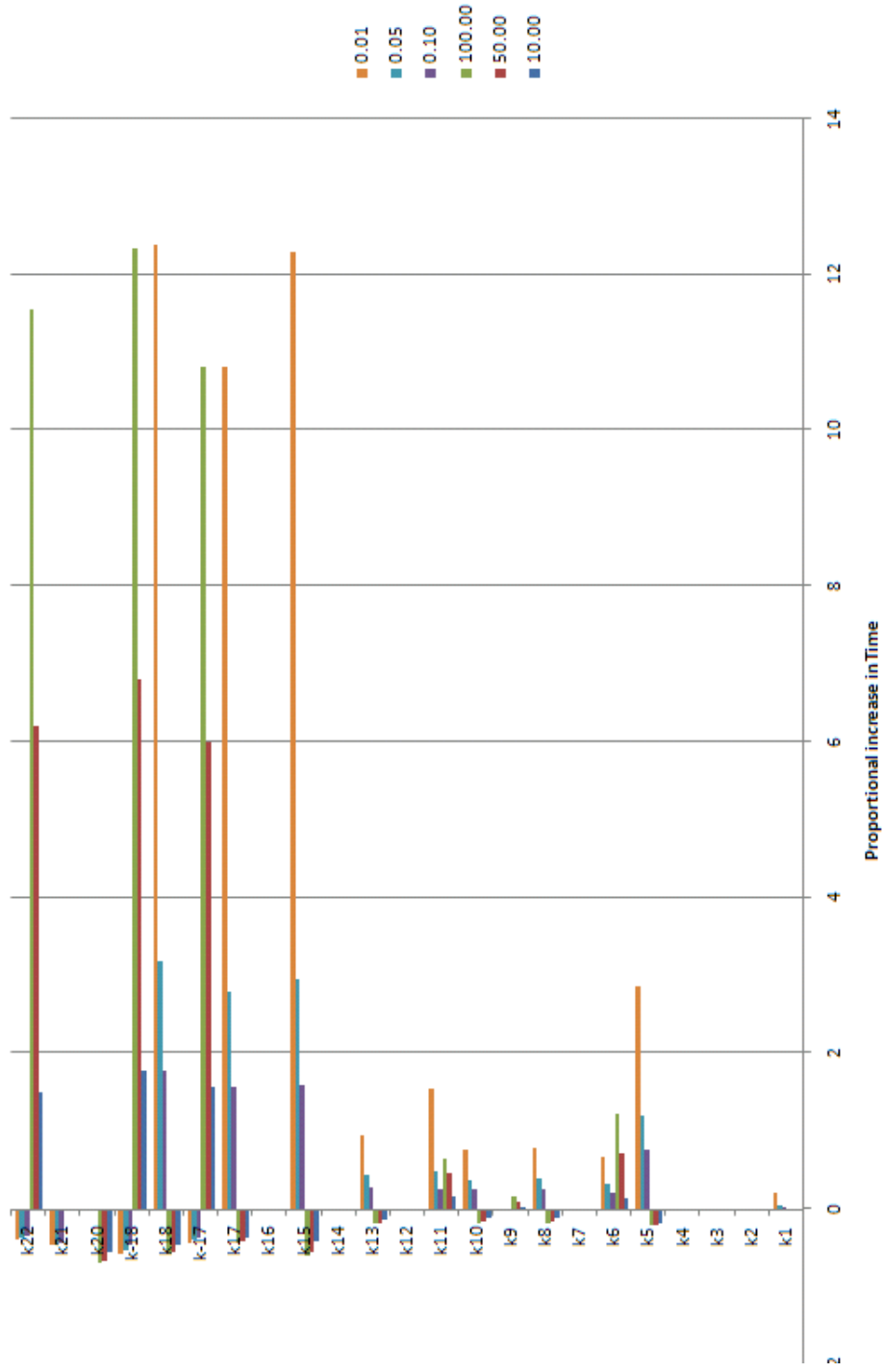
Figure 3.4: Graph showing affect of changing rate constants on model output, with k_{19} removed
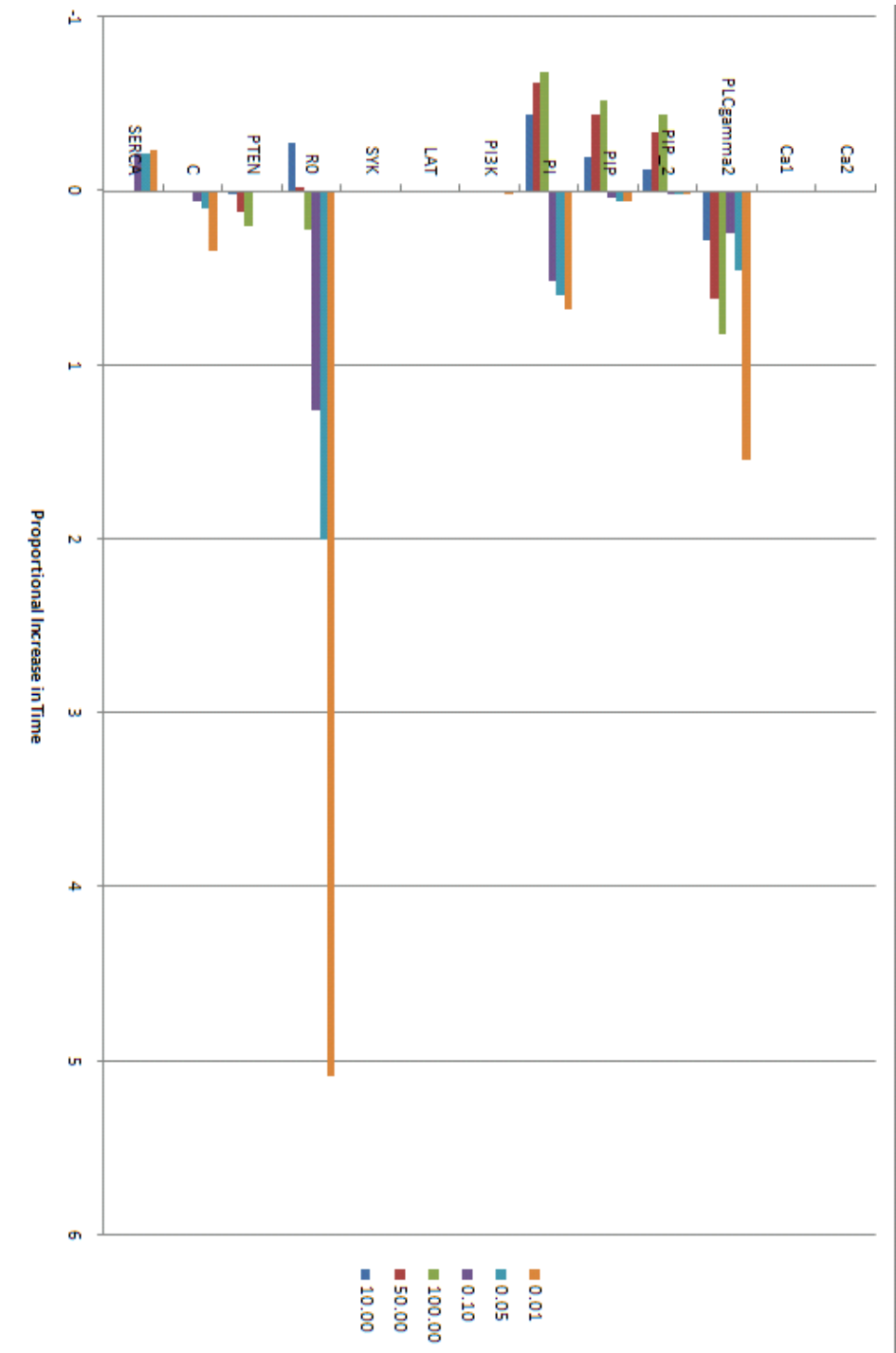
Figure 3.5: Graph showing affect of changing initial concentrations on model output

the system of equations

$$0 = -\bar{k_{17}}\widehat{P} + \bar{k_{-17}}\widehat{P_1} + \bar{k_{21}}\widehat{D}\widehat{I} \tag{3.12}$$

$$0 = \bar{k_{17}}\widehat{P} - \bar{k_{18}}\widehat{P_1} - \bar{k_{-17}}\widehat{P_1} + \bar{k_{-18}}\widehat{P_2} \tag{3.13}$$

$$0 = -\bar{k_8}\widehat{v_3}\widehat{P_2} + \bar{k_9}\widehat{P_3}\widehat{P_{10}} - \bar{k_{15}}\widehat{v_7}\widehat{P_2} - \bar{k_{16}}\widehat{v_8}\widehat{P_2}$$
$$+\bar{k_{18}}\widehat{P_1} - \bar{k_{-18}}\widehat{P_2} \tag{3.14}$$

$$0 = \bar{k_8}\widehat{v_3}\widehat{P_2} - \bar{k_9}\widehat{P_3}\widehat{P_{10}} \tag{3.15}$$

$$0 = \bar{k_{15}}\widehat{v_7}\widehat{P_2} + \bar{k_{16}}\widehat{v_8}\widehat{P_2} - \bar{k_{21}}\widehat{D}\widehat{I} \tag{3.16}$$

$$0 = \bar{k_{20}}(\widehat{I_T} - \widehat{I_{RC}})(\widehat{Ca_T} - \widehat{Ca_2}) - \bar{k_{22}}\widehat{Ca_2}S^A \tag{3.17}$$

to solve.

We can see from numerical results that $I_{RC} = 0$ at steady state, which means from equation (3.17) we find

$$\widehat{Ca_2} = \frac{\bar{k_{20}}\widehat{I_T}\widehat{Ca_T}}{\bar{k_{20}}\widehat{I_T} + \bar{k_{22}}\widehat{S^A}} \tag{3.18}$$

with the equations (3.12) – (3.16) giving us the relations

$$\widehat{P} = \frac{(\bar{k_{-17}} + \bar{k_{18}})\widehat{P_1} + \bar{k_{-18}}\widehat{P_2}}{\bar{k_{17}}} \tag{3.19}$$

$$\widehat{D} = \frac{\bar{k_{18}}\widehat{P_1} + \bar{k_{-18}}\widehat{P_2}}{\bar{k_{21}}\widehat{I}} \tag{3.20}$$

$$\widehat{v_3} = \frac{\bar{k_9}\widehat{P_3}\widehat{P_{10}}}{\bar{k_8}\widehat{P_2}} \tag{3.21}$$

$$\widehat{v_7} = \frac{(\bar{k_{18}} - \bar{k_{16}}\widehat{v_8})\widehat{P_2} + \bar{k_{18}}\widehat{P_1}}{\bar{k_{15}}\widehat{P_2}}. \tag{3.22}$$

From equation (3.18) we can find the steady state of $Ca^{(2)}$ from initial concentrations. Equations (3.19)–(3.22) however, tell us little due to the

amount of variables involved. We could approximate the steady state of the lipids PI, PIP and PIP_2 by their initial concentrations as it can be seen from Figure (3.2) their steady states differ little from this. This would reduce the number of variables an may give us more useful relations.

3.5   Comparison to Experimental Data

In Figure (3.6) we can see our model compared to experimental data provided by Dr. Chris Jones. Comparing the two sets of data we find that our model takes longer to produce the calcium rise. Although our model qualitatively models the actual rise in calcium well, we do not then get the reduction to a steady state as is shown in the experimental data. This could be due to the lack of inhibition and backward reactions within our model reducing the amount of calcium release from the DTS over time.
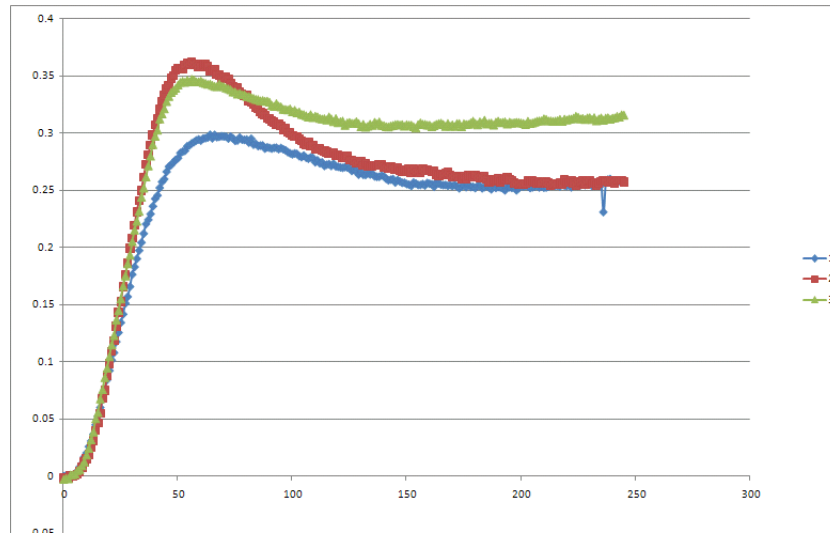
(a)
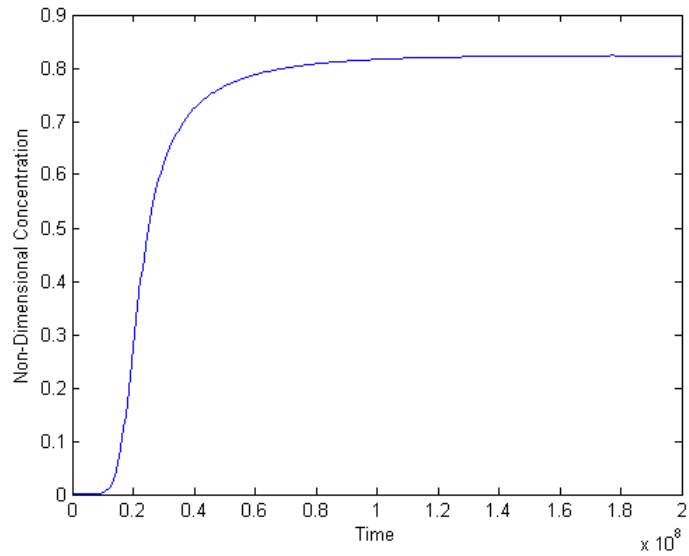
(b)

Figure 3.6: Graphs showing (a) experimental calcium in cytosol over time and (b) model calcium in cytosol over time.

Chapter 4

Conclusions and Discussion

This dissertation has formulated and solved a model for the collagen–GPVI pathway. We found the model transfers calcium from the DTS to the cytosol as required. We carried out a sensitivity analysis of this model finding k_{20}, which is the rate directly effecting calcium transfer to have a great influence. In addition we found concentrations and rate constants connected to the lipid cycle being influential in the model as well as k_5, the rate constant before Figure (2.2) can be seen to branch in two.

The first model, however, had some problems. It emptied the DTS of calcium, as well as having the problem of IP_3 and DAG not reaching steady states. An improved model was formulated, including the recycling of IP_3 and DAG into PI and the movement of calcium back into the DTS. Sensitivity analysis of this model found very similar influential parameters to that of the first model. However k_{22} now becomes less significant, the concentration of $SERCA$ as well as the rate constant k_{22} have a more than average affect on the model.

Comparing to experimental data we find that although calcium in the cytosol rises in our model, it takes much longer. We also find that the behaviour of our calcium level doesn't match the experimental data which

exhibits a rise and a small fall.

The technique we used to form our model was one which modelled the whole pathway at once. Another way would have been to separate the pathway into module, as in [12]. The advantages this would have given us is that we could more accurately study each part of the pathway, and the affect of parameter changes within the modules. The problem may have been fitting the pathway together after this as though a enclosed module may work well enough on its own, it may not work in the context of the whole pathway once connected with others.

4.1 Future Work

Our model only considers forward reactions, although all the reactions in our model are reversible. The inclusion of backward reactions in our model may produce a more realistic calcium behaviour. We could also include inhibition as in [12].

The majority of the parameters within our model have been assumed. To make the model work more accurately it would be advisable to do a literature search to find reliable values for all rate constants and initial concentrations.

Extension of the pathway may also be possible. We may wish to add other parts of the pathway featured in Figure (2.1) or possibly some of the modules in [12]. We could also increase the pathway past calcium to include secretion of thrombin.

We also assumed in this model that the platelet is spatially heterogeneous. This is not the case in actual platelets, this means we could add to our model a spatial aspect. This would mean using partial differential equations as opposed to ordinary differential equations. A stochastic model could also possibly be used.

Bibliography

[1] AMERICAN HEART ASSOCIATION. Venous thromboembolism and pulmonary embolism – statisitics. www.americanheart.org/downloadable/heart/1200598191688FS29VTE08.pdf.

[2] BARRETT, N., HOLBROOK, L., JONES, S., KAISER, W., MORAES, L., RANA, R., SAGE, T., STANLEY, R., TUCKER, K., WRIGHT, B., AND GIBBINS, J. Future innovations in anti-platelet therapies. *Br. J. Pharmacol. 154* (2008), 918–939.

[3] FAEDER, J., HLAVACEK, W., REISCHL, I., BLINOV, M., METZGER, H., REDONDO, A., WOFSY, C., AND GOLDSTEIN, B. Investigation of early events in fcεri–mediated signaling using a detailed mathematical model. *J. Immunol. 170* (2003), 3769–3781.

[4] GIBBINS, J. Platelet adhesion signalling and the regulation of thrombus formation. *J. Cell Sci. 117* (2004), 3415–3415.

[5] HAFEZ, S. A computational model of glycoprotein VI receptor signalling pathway in platelets. *M.Sc. in Research Methods in Cell Biology, 2007 School of Biological Sciences, The University of Reading* (2003).

[6] IHEKWABA, A., BROOMHEAD, D., GRIMLEY, R., BENSON, N., AND KELL, D. Sensitivity analysis of parameters controlling oscillatory sig-

nalling in the nf-κb: the roles of ikk and iκbα. *Sys. Biol. 1* (2004), 93–103.

[7] LeVeque, R. *Finite Difference Methods for Ordinary and Partial Differential Equations*. SIAM, 2007.

[8] Miura, Y., Takahashi, T., Jung, S., and Moroi, M. Analysis of the interaction of platelet collagen receptor glycoprotein vi (gpvi) with collagen. *J. Biol. Chem. 277*, 48 (2002), 46197–46204.

[9] Morbiducci, U., Ponzini, R., Nobili, M., Massai, D., Montevecchi, F., Bluestein, D., and Redaelli, A. Blood damage safety of prosthetic heart valves. shear-induced platelet activation and local flow dynamic: A fluid–structure interaction approach. *J. Biomech.* (2009).

[10] Murray, J. *Mathematical Biology I: An Introduction*. Springer, 2004.

[11] Pivkin, I., Richardson, P., and Karniadakis, G. Blood flow velocity effects and role of activation delay time on growth and form of platelet thrombi. *PNAS 103* (2006), 17164–17169.

[12] Purvis, J., Chatterjee, M., Brass, L., and Diamond, S. A molecular signaling model of platelet phosphoinositide and calcium regulation during homeostasis and P2Y1 activation. *Blood 112* (2008), 4069–4079.

[13] Suzuki, H., Murasaki, K., Kodama, K., and Takayama, H. Intracellular localization of glycoprotein VI in human platelets and its surface expression upon activation. *Br. J. Haematol. 121*, 6 (2003), 904–912.

[14] Xu, C., Zeng, Y., and Gregersen, H. Dynamic model of the role of platelets in the blood coagulation system. *Med. Eng. Phys. 24* (2002), 587–593.

[15] Xu, Z., Chen, N., Kamocka, M., Rosen, E., and Alber, M.
     A multiscale model of thrombus development. *J. R. Soc. Interface 5*
     (2008), 705–722.